surfaces

MDPI

Review

Catalysis Mediated by 2D Black Phosphorus Either Pristine or Decorated with Transition Metals Species

Matteo Vanni [1,2], Maria Caporali [1,*], Manuel Serrano-Ruiz [1] and Maurizio Peruzzini [1]

[1] CNR ICCOM, Via Madonna del Piano 10, 50019 Sesto Fiorentino, Italy; mvanni@iccom.cnr.it (M.V.); mserrano@iccom.cnr.it (M.S.-R.); mperuzzini@iccom.cnr.it (M.P.)

[2] Department of Biotechnology, Chemistry and Pharmacy, Via Aldo Moro 2, 53100 Siena, Italy

* Correspondence: maria.caporali@iccom.cnr.it

Received: 4 February 2020; Accepted: 13 March 2020; Published: 1 April 2020

Abstract: Among the novel class of mono-elemental two-dimensional (2D) materials, termed Xenes, phosphorene is emerging as a great promise for its peculiar chemical and physical properties. This review collects a selection of the recent breakthroughs that are related to the application of phosphorene in catalysis and electrocatalysis. Noteworthy, thanks to its intrinsic Lewis basic character, pristine phosphorene turned out to be more efficient and more selective than other non-metal catalysts, in chemical processes as the electroreduction of nitrogen to ammonia or the alkylation of nucleophiles with esters. Once functionalized with transition metals nanoparticles (Co, Ni, Pd, Pt, Ag, Au), its catalytic activity has been evaluated in several processes, mainly hydrogen and oxygen evolution reactions. Under visible light irradiation, it has shown a great improvement of the activity, demonstrating high potential as a photocatalyst.

Keywords: phosphorene; 2D Materials; electrochemistry; catalysis; late transition metals

1. Introduction

The wide field of two-dimensional (2D) materials chemistry, which in the last fifteen years has grown and developed, offers new opportunities in heterogeneous catalysis. For many aspects, bidimensional materials have unique advantages over three-dimensional (3D)-bulk catalysts. First, being made by stacking of single to few monolayers, 2D materials approach the limit of searching for a high specific surface area, meaning a high density of active sites, which is in itself relevant for a catalyst to be effective. Second, the electronic properties of 2D materials are strongly correlated to the flake morphology. This means that variation in layer thickness, lateral dimensions, the presence of defects on the surface (vacancies or dislocations), or just its chemical modification may all have a dramatic impact on material's properties, like band gap, density of states, or electrical and thermal conductivities. Thus, it is not surprising that these changes may, in turn, influence the catalytic performance of the material. It is also relevant that the surface homogeneity of 2D materials as compared to 3D-catalytic systems make it easier, at least in principle, to tackle the problem of surface characterization (i.e., via commonly available HRTEM or atomic force microscopy (AFM) techniques) and its computational modelling. This provides the opportunity to combine experimental and theoretical approaches to devise and implement new catalysts and rationalize their catalytic mechanism. After the explosion of this research area, with the growth of graphene chemistry, increasing bidimensional materials have been prepared and characterized. Nowadays, it is currently possible to distinguish between elemental 2D materials (borophene, graphene, phosphorene, antimonene, etc.) [1] or polynuclear compounds, such as hexagonal-boron nitride (*h*-BN), transition metal dichalcogenides (MX_2) [2], the so-called MXenes (transition metals carbides, nitrides, and carbonitrides) [3], 2D alloys [4], and many others. Phosphorene, as has been called the monolayer that was obtained from the exfoliation of black

phosphorus crystals, is the 2D material that has, so far, received more attention beside graphene. As dealing with a genuine single layer of black phosphorus is extremely unlikely, and since all catalytic application rely on flakes containing more than one layer, from now on we prefer to use the acronym 2D BP to address the exfoliated material.

Elemental phosphorus does exist in different allotropic forms, all named according to their colour, which ranges from the molecular allotrope white phosphorus, made of P_4 tetrahedra, to polymeric forms, such as red, violet, and black phosphorus. The latter represents the thermodynamically most stable and less noxious form of the element. Despite being known for a long time (its first description dates back to 1914 [5]) black phosphorus remained scarcely considered until 2014, when a sudden and rapidly growing interest started to arise around this material following its reported exfoliation [6,7]. This was largely due to the unique electronic and optical properties of the material, as both theoretical and experimental studies revealed that black phosphorus is a semiconductor with a tunable, layer-dependent bandgap, going from 0.3 eV in the bulk material to about 2.0 eV in the monolayer. This enables light absorption in a wide range of frequencies that range from ultraviolet light to visible light, and even near-infrared light, opening up potential applications in optoelectronic devices, photovoltaics, [8] energy storage, and photocatalysis [9]. Furthermore, black phosphorus possesses a large on/off ratio and high charge carrier mobility that is 1000 $cm^2\ V^{-1}\ s^{-1}$ at ambient temperature and rise up to 6000 $cm^2\ V^{-1}\ s^{-1}$ at lower temperature, much larger than in transition metal dichalcogenides (≈300 $cm^2\ V^{-1}\ s^{-1}$) [10,11]. The structure of black phosphorus is reminiscent of graphene's one, which is based on the repetition inside each layer of a six-membered ring. However, unlike graphene, which is made of sp^2 carbon atoms, the sp^3 hybridization of phosphorus forces each P_6-ring to a chair conformation. Thus, the monolayer of black phosphorus is puckered, with an alternation of ridges and valleys, which enables the distinction of two non-equivalent directions in the layer, an armchair direction (AC), and a zig-zag direction (ZG) (see Figure 1). As a result of this atomic structure, a negative Poisson's ratio has been calculated for monolayer BP, and this intrinsic property imparts unique mechanical characteristics to the material, since most of the materials are endowed with a positive Poisson's ratio, i.e., once they are stretched longitudinally, their lateral dimension diminishes [12].

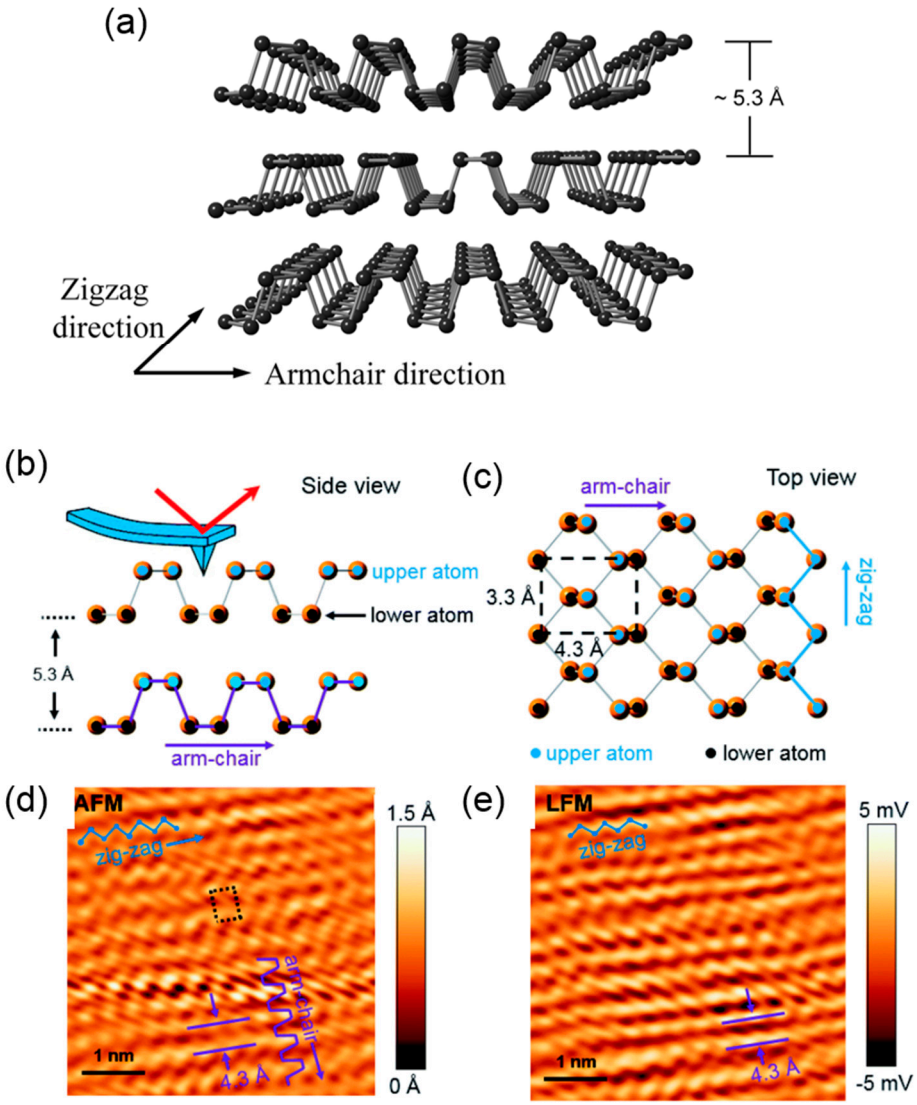

Figure 1. (**a**) Atomic structure of multi-layer black phosphorus. Reprinted with permission from ref. [13]. Copyright 2015 Royal Society of Chemistry. Characterization of freshly cleaved black phosphorus. (**b**) Side and (**c**) top views of puckered layered crystal structure of black phosphorus. The interlayer distance is 5.3 Å. The crystal layer has a 4.3 Å periodic armchair pattern and 3.3 Å periodic zig–zag pattern, as indicated by the dashed rectangle in (**c**). A monolayer of BP is composed of upper atoms (marked by blue dots) and lower atoms (marked by black dots). (**d**) Atomically resolved atomic force microscopy (AFM) and (**e**) lateral force microscopy (LFM) images of BP for a scan size of 5 × 5 nm^2. Both of the images show the zig–zag pattern and 4.3 Å periodic armchair structure. The rectangular unit cell of BP is marked by the black dotted line in (**d**). Reprinted from ref. [14]. Copyright 2020 Royal Society of Chemistry.

The puckered structure imparts a strong in-plane anisotropy, which is absent in graphene, to black phosphorus, which is reflected in anisotropic thermal and electric properties.

These unique optical, electronic, and mechanical properties of BP aroused great interest among scientists, allowing for the design of new functional BP-based electronic devices [15]. In particular, BP has been applied in the realization of high performance field effect transistors (FETs). Although most of the studies have focused on the basic electronic characterization of the devices, BP-based FETs have been successfully applied for sensing [16–18] or photodetection. [19–21]

Thanks to the very low cytotoxicity of black phosphorus in comparison to other 2D materials as graphene and transition metals dichalcogenides [22], and to its photonic properties, the application of BP in the biomedical field has grown exponentially, as recently reviewed by Qu G. and co-workers [23]. The seminal work conducted by Xie Y. et al. [24] demonstrated that BP nanosheets are stable in water for a certain time and they can generate efficiently singlet oxygen under the entire visible light region, thus opening the application of BP not only in photocatalysis, but also in photothermal and photodynamic therapy (PDT). When compared to other PDT agents, BP has the advantage to be biodegradable, since its degradation/oxidation produces phosphates that are already present in the human body as a component in bone tissues. Thus, BP also represents a good candidate for regenerative medicine [25]. Furthermore, BP has also demonstrated great potential in biosensing, controlled drug release, and antibacterial use [23]. The sp^3 hybridization of phosphorus atoms in BP is also responsible for the presence of a lone pair on each atom. Theoretical calculations have shown how the Lewis-basicity of black phosphorus is less than that of molecular phosphines, owing to an unfavorable combination of steric and electronic effects [26]; nonetheless, the naïve description of 2D BP as an extended polydentate ligand is irresistibly fascinating for a chemist and it provides a useful conceptual model toward its chemical functionalization, especially with metal units. Furthermore, the ability of 2D BP to form coordinative bonds with transition metals with bond-lengths that are even close to those found in some phosphine complexes has already been experimentally demonstrated in a 2D BP/Pd system (see Section 5.3).

2. Synthesis and Exfoliation of Black Phosphorus

The first preparation of black phosphorus dates back to 1914, when physicist Percy Bridgman [5] serendipitously prepared this new allotropic form under high-pressure conditions, working at 1.2 GPa and approximately 200 °C. The first low pressure synthesis was much later reported in the 1960s and further improved in the 1980s [27], when black phosphorus was obtained by recrystallization from a melt of white phosphorus in liquid bismuth at 300–400 °C. However, by this procedure, the obtained crystals were needle-shaped and smaller than those that were prepared by high pressure routes. An important step forward was made in 2007 by T. Nilges et al. [28], who prepared black phosphorus starting from the red allotrope via the chemical vapor transport. An AuSn alloy promoted the reaction, while SnI_4 was used as the mineralizing agent. A mixture of these ingredients and red phosphorus were sealed in an evacuated quartz tube and then heated at 650 °C for three days. This synthetic protocol has been crucial for the subsequent development of 2D BP chemistry, since the purity, dimensions, and crystallinity of the material obtained is suitable for both the mechanical and liquid exfoliation. In 2014, this protocol was further improved, enabling the use of Sn and SnI_4 as mineralizers, avoiding the use of expensive Au [29]. In the same year, the group of Y. Zhang et al. [6] and Peide Ye and his co-workers [7] independently reported the first exfoliation of black phosphorus crystals, which was performed by a classical scotch-tape method, as had been done previously with graphite. This marked the birth of a new research field that has grown rapidly in the following years and it is still continuing to expand at a significant rate. While mechanical exfoliation is appropriate for building electronic devices while using a single 2D BP flake (e.g., to make transistors), a large scale exfoliation method is necessary in order to employ 2D BP as a catalyst or as platform to support a catalytic species. Among the different procedures developed so far, liquid phase exfoliation (LPE) remains the most commonly employed in the context of chemistry and related applications. With this method, black phosphorus crystals, being suspended in a solvent, having a high boiling point, and a high dielectric constant, are disrupted and exfoliated through the action of ultrasounds (see Figure 2).

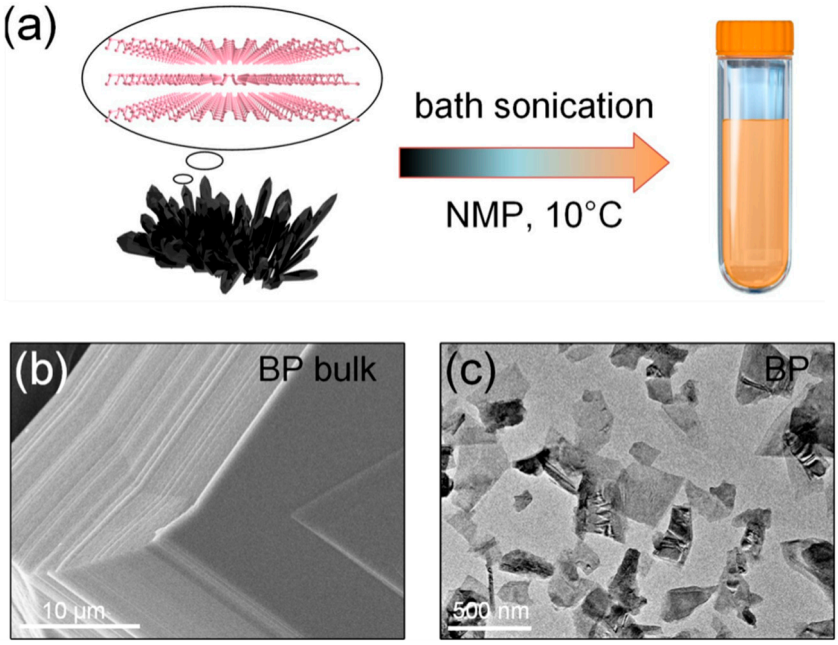

Figure 2. (**a**) Typical black phosphorus (BP) exfoliation procedure in N-methylpyrrolidone (NMP). (**b**) TEM image of bulk BP crystals before the exfoliation and (**c**) exfoliated material (2D BP). Reprinted with permission from ref. [30]. Copyright 2018 Wiley.

The role of the solvent goes beyond being a simple medium for the propagation of ultrasounds, as it plays a crucial role in stabilizing the exfoliated 2D BP flakes with energetically favourable interactions, allowing for an effective separation of the layers from the crystal. *N*-methylpyrrolidone (NMP) is the most used LPE-solvent, but other solvents, like dimethyl sulfoxide (DMSO), may afford excellent exfoliated material, both in terms of lateral flake dimensions and flake thickness [31].

Ambient Stability of Exfoliated Black Phosphorus

Meanwhile, bulk black phosphorus is relatively stable in ambient conditions, the exfoliated few-layer BP (2D BP) is reactive towards water and oxygen forming molecular compounds as phosphorus oxides and acids. The lattice structure of BP is than altered and, consequently, also its chemical and electronic properties, preventing its application in devices and in all processes carried out in ambient conditions. Several studies have addressed such fundamental issues, and various routes have been proposed to avoid oxidation [32]. For instance, the encapsulation of 2D BP is an effective tool for preventing oxidation and it has been achieved either sandwiching it with inert 2D materials as graphene or *h*-BN forming heterostructures, or by coating with Al_2O_3 through the ALD technique [33]. Other passivation strategies include the functionalization of the surface by the adsorption of organic molecules [34,35], transition metals [36], ionic liquids [37], or highly hydrophobic polymers [38], just to cite a few. The mechanism by which the oxidation goes through is still an open debate, though some first-principle studies have been published [32].

3. Chemisorption Studies on Exfoliated Black Phosphorus

Many catalytic processes, especially those addressing the activation of small molecules, involve gases as reacting species. Wishing to investigate the application of BP in catalysis, it is of paramount importance to understand the interaction between the surface of BP and adsorbed gas species. BP has different possible adsorption sites thanks to its puckered anisotropic structure [39,40]. This interaction might range from a weak physisorption to a reactive adsorption, depending on the particular gas considered and its inherent reactivity. Oxygen was immediately recognized to slowly react with BP

and this indeed is the main factor limiting the stability of BP upon air exposure (see Section 2). Y. Huang et al. modelled the interaction of O_2 with monolayer-BP (1L-BP) by DFT calculations [41]. The physisorbed O_2 molecule turned out to be slightly favoured when compared to the free molecule, however this state is only metastable and easily undergoes exothermic dissociative adsorption, with formation of P–O bonds. Searching for applications of BP in gas sensing, L. Kou et al. performed first principle calculations on several typical small gas molecules, i.e., CO, CO_2, NH_3, NO, and NO_2 [39]. Among these, NO and NO_2 turned out to have the strongest interaction with 1L-BP. In particular, NO is chemisorbed on the surface forming a direct P–N bond, accepting electron density from BP. NO_2 also behaves as an electron acceptor, resulting in a strong adsorption, though without direct bonding to phosphorus. Such appreciable interaction with NO_2 was exploited by A.N. Abbas et al., who realized the first BP-based sensor toward this molecule [42]. Carbon based gases, such as CO and CO_2, were shown to only interact weakly with BP, with CO having the least adsorption energy among the investigated molecules. Surface functionalization is the preferred method for introducing new active sites for gas adsorption on a given material, in order to enhance or inhibit the affinity for a chosen gas species. In this regard, S. Y. Lei et al. studied the adsorption of CO on 1L-BP decorated with metal ad-atoms, showing that the CO adsorption capacity could be tuned by DFT calculation by varying the type and amount of surface modifier [43]. Although the latter theoretical investigation regarded the use of single metal atoms as functionalizing agents, undoubtedly similar effects may be obtained with metal nanoparticles. P. Yasaei et al. followed a similar approach, who used Pt nanoparticles to decorate BP aiming to fabricate a H_2-sensor [44]. This functionalization successfully overcomes the negligible interaction with H_2 being observed in unmodified BP.

4. Catalytic Applications of Pristine Black Phosphorus

Some of the biggest chemical productions worldwide are realized while using metal based-heterogeneous catalysts. Ammonia has been produced since 1913 through the Haber–Bosch process, with an iron oxide catalyst [45,46]. Gasoline is made via Fischer–Tropsch synthesis, where carbon monoxide and hydrogen are converted into liquid hydrocarbons employing catalysts that are based on Co, Fe, or Ru [47,48]. Crude and refined oil, as well as natural gas, are cleaned from sulfur and other contaminants by hydrodesulfurization processes, which rely on cobalt and molybdenum catalysts that are supported on Al_2O_3 [49]. Catalytic reforming of cyclic alkanes is carried out on Pt-based systems to convert such feedstock into aromatic chemicals and branched alkanes [50]. Electrolytic hydrogen is industrially generated at the surface of Pt-electrocatalysts and many other examples could be cited. The use of metal-based systems stems from the wide ability of transition metals and their compounds to interact and activate small molecules or functional groups. Metal-free heterogeneous catalysts are more rare and are usually based on graphitic carbon nitride or other carbon-based material [51] (i.e., reduced graphene oxide, carbon nanotubes, fullerene). However, active sites that are able to both bind the target substrate and activate it toward a partner reagent are rare to find in pristine materials; therefore, surface functionalization is mandatory. BP is an outstanding exception to the rule, as even the pristine material possesses intriguing characteristics, which may come into play at different stages of a catalytic cycle. Indeed, BP is able to interact with molecular systems with delocalized electrons through weak van der Waals interactions. These physisorption interactions are intrinsically different from those observed, for example, with graphene. The latter, given the sp^2 hybridization of carbon and the electronic delocalization on the layer, gets involved easily in the weak interaction of π–π type, which arises from the mutual attraction of π-electron densities both present in graphene and in the physisorbed molecule. In contrast, black phosphorus is characterized by an sp^3 hybridization and weak Lewis-basicity. The interaction between black phosphorus and the π-system of the adsorbed molecules is better described in terms of polarization of the phosphorus atoms' lone pair, which is partially donated to the empty π^* orbitals of the adsorbate. Such an interaction has been theoretically described and even experimentally exploited to achieve a non-covalent functionalization of black phosphorus [34,52]. Moreover, besides interacting with conjugated systems, the Lewis-basicity

of BP makes it possible to anchor Lewis-acidic species at its surface. Even if most applications that are reported in this field make use of surface modified black phosphorus (see Section 5), it has been demonstrated that pristine black phosphorus itself might be catalytically active in some relevant chemical and electrochemical processes.

4.1. HER and OER Processes

Our society is currently struggling in the search of renewable energies. Hydrogen, as an energy vector, could be, in principle, a possible solution to overcome the dependence from fossil fuels. Electrochemical water splitting represents one of the most convenient and promising approaches to hydrogen generation, although the catalysts used nowadays for this process are based on noble metals, such as Pt and Pd [53,54]. Due to their scarcity and high cost, the current challenge is to use cheap and relatively abundant metals, or avoid at all the use of a metal, moving the choice towards more environmentally friendly materials. In this way, the prospective of the commercial application of fuel cells and water splitting on a large scale will become feasible [9]. Pumera M. et al. were the first to show how pristine black phosphorus might successfully promote the hydrogen evolution reaction (HER) [55]. A glassy carbon electrode (GCE) was coated with dropcasted 2D BP nanoflakes and the resulting current that was associated to H^+ reduction was evaluated by linear sweep voltammetry and electrochemical impedance spectroscopy. It is noteworthy that 2D BP used in this study was nanometric in size (i.e., 2D BP nanoparticles having size lower than 100 nm), being prepared through an electrochemical exfoliation procedure. A potential difference of 10 V was applied between two platinum electrodes dipped inside a suspension of BP microcrystals. In this way, potential differences were induced at the opposite side of each crystal, which led to its fragmentation (see Figure 3). By this method, 2D BP nanoflakes with an average lateral dimension of 70 nm were obtained.

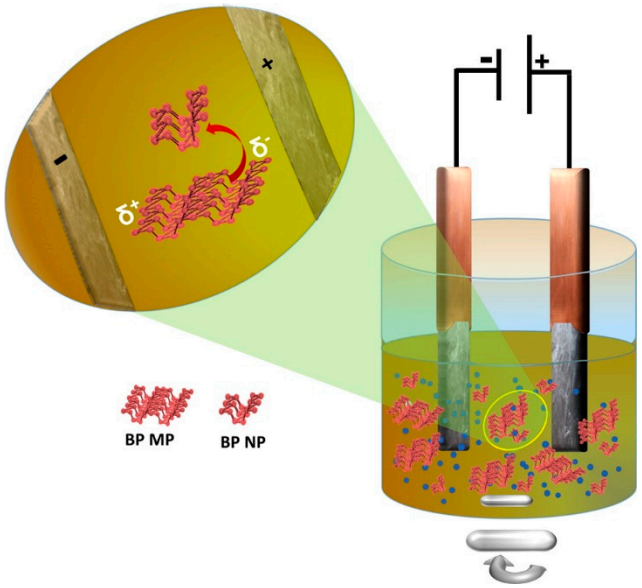

Figure 3. Experimental set-up for the electrochemical exfoliation of bulk BP crystals. Reprinted with permission from ref. [55]. Copyright 2016 American Chemical Society.

Electrochemical measurements revealed how flake dimension is crucial in affecting pristine 2D BP activity in hydrogen evolution. Indeed, 2D BP nano-flakes outperformed the 2D BP micro-flakes that were used for comparison (see Figure 4).

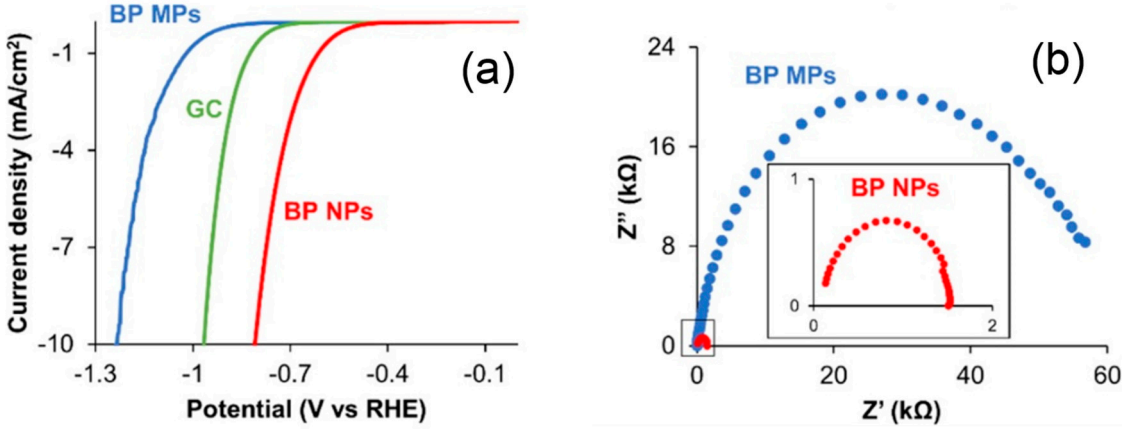

Figure 4. Linear scan voltammograms (**a**) and Nyquist plots (**b**) of black phosphorus macroparticles (BP MPs) and black phosphorus nanoparticles (BP NPs) in 0.5 M H_2SO_4. Reprinted with permission from ref. [55]. Copyright 2016 American Chemical Society.

Yang S. and co-workers achieved an important step forward, who, for the first time, studied the photocatalytic H_2 evolution of BP nanosheets under visible light [56]. Exfoliated BP was prepared by the ball-milling of the bulk precursor in the presence of LiOH as additive, which induced the functionalization with hydroxyl (OH) groups of BP edges. This functionalization turned out to be crucial, since, in the absence of it, bare BP nanosheets resulted in being unstable in the reaction conditions and it hampered the hydrogen production. Noteworthy, without using any noble metal co-catalysts, it reached a hydrogen evolution rate up to 512 μmol h^{-1} g^{-1}, which is 18 times higher than bulk BP, and it is comparable or even higher than graphitic carbon nitrides (g-C_3N_4). On the basis of spectroscopic investigation, it was revealed that passing from bulk BP down to few-layer BP, there is a negative shift of the conduction band and a positive shift of the valence band, which leads to a dramatic increase of energy band gap, as shown in Scheme 1. In detail, the more negative potential of the conduction band of BP-BM in comparison to the redox potential of H^+/H_2 enhances its electron reduction ability, and the generated holes at the valence band level can react with S_2^-/SO_3^{2-}, thus inhibiting the electron-hole recombination. In agreement with theoretical calculations [57], the much higher activity of exfoliated BP as photocatalyst, being assisted also by the increased surface area with respect to the bulk counterpart, was experimentally demonstrated.

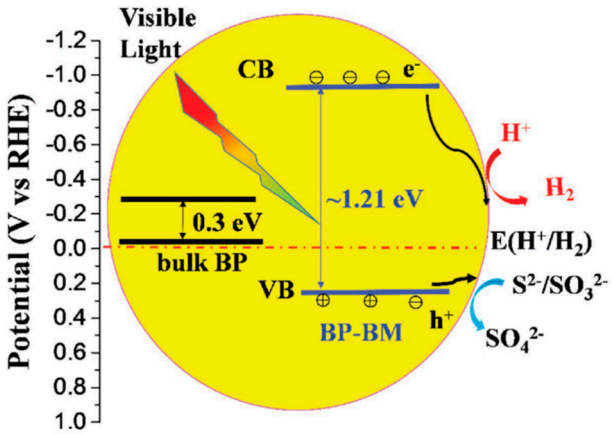

Scheme 1. The mechanism of the photocatalytic hydrogen evolution of bulk BP and BP-BM, where the latter is BP functionalized with hydroxyl groups. Reprinted with permission from ref. [56]. Copyrights 2017 John Wiley and Sons.

Afterwards, S. K. Muduli et al. studied the evolution of hydrogen from pristine BP under visible light illumination [58], preparing both 2D BP nanosheets and nanoparticles while using a liquid phase exfoliation procedure that was carried out in *N*-methyl-2-pyrrolidone. Varying the exfoliation conditions (i.e., sonication power, time, and temperature), 2D BP nanosheets with lateral dimension of about 1 µm and ~8 layers-thickness were obtained, meanwhile BP nanoparticles showed a mean diameter of ~5 nm. The exfoliated material was tested as a photocatalyst for hydrogen evolution from water, while using triethanolamine as the sacrificial agent under visible light irradiation. Continuous H_2 evolution was observed with both 2D BP nanosheets and nanoparticles over a period of 40 h, demonstrating the potential application of the pristine material, without any added surface modifier, as an effective photocatalyst under VIS irradiation. Additionally, the DFT calculations predicted that H_2 evolution of bilayer BP is independent from the edge or center positions, which is a unique property of this material that we do not find in other 2D companions.

In a seminal work by You H. et al., [59] it was discovered that 2D BP is a pyroelectric material and this physical property can be of great advantage in catalysis. Indeed, it was shown that 2D BP, once suspended in water in the dark, can afford a direct hydrogen evolution of approximately 540 µmol h^{-1} per gram of catalyst, after 24 thermal cycling between 15° C and 65° C. The reason behind it is that the cold-hot alternation excitation induces a net change of the electric dipole moment in the material, thus positive and negative charges are created. The charges will transfer from the surface of BP to the molecules of the reagents, allowing for the redox reaction to take place. These results open new avenues in the application of 2D BP as pyrocatalyst, not only for the HER process. The current protocol by You H. et al. [59] can be improved by also exploiting the photocatalytic activity of BP, which, in synergy with the capacity of heat energy harvesting, might greatly enhance the production rate of hydrogen from water.

Further improvements in the HER process have been achieved using surface functionalized 2D BP, in particular with platinum and gold nanoparticles, as will be discussed in Sections 5.4 and 5.6 respectively.

S. Wang and collaborators [60], who grew nanocrystalline BP on a titanium foil using a thermal-vaporization transformation, reported the first application of BP in the complementary oxygen evolution reaction (OER). In detail, red phosphorus crystals were heated in a tube furnace at 650 °C in the presence of titanium support under an argon flow. By this method, the surface of titanium was covered with a uniform texture of crystalline BP (see Figure 5).

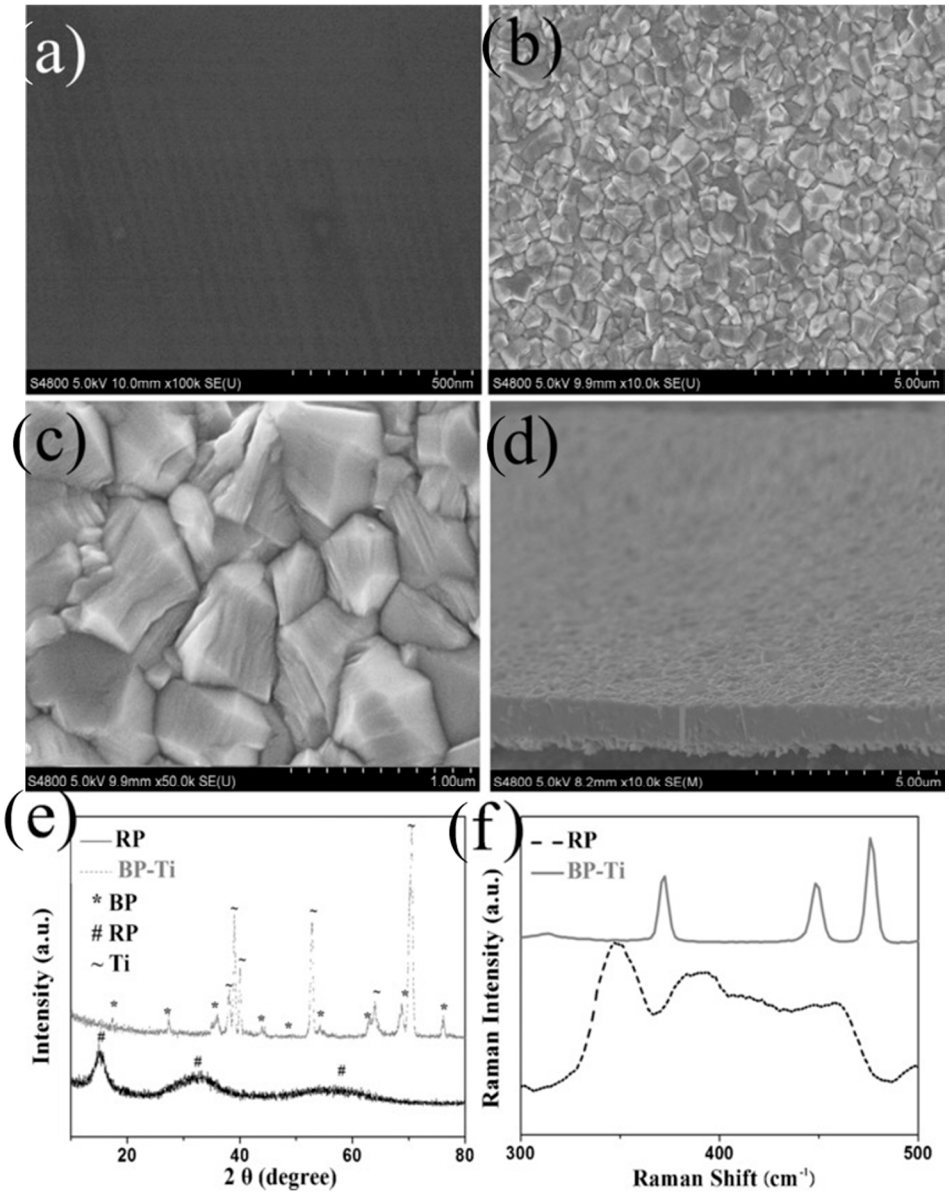

Figure 5. (**a**) SEM image of Ti foil (**b**), (**c**) SEM images of BP-Ti (**d**) Cross-section of BP-Ti (**e**) XRD patterns and (**f**) Raman spectra of BP-Ti and red phosphorus. Reprinted with permission from ref. [60]. Copyright 2016 John Wiley and Sons.

The resulting BP–Ti foil was tested as a working electrode in the OER while using an alkaline medium. The material turned out to have good activity in the process, with an onset potential of 1.48 V, which was comparable to the values of many oxide-based electrocatalysts used in OER (see Figure 6). These results should be ascribed to the presence of BP, since bare titanium turned out to be inactive.

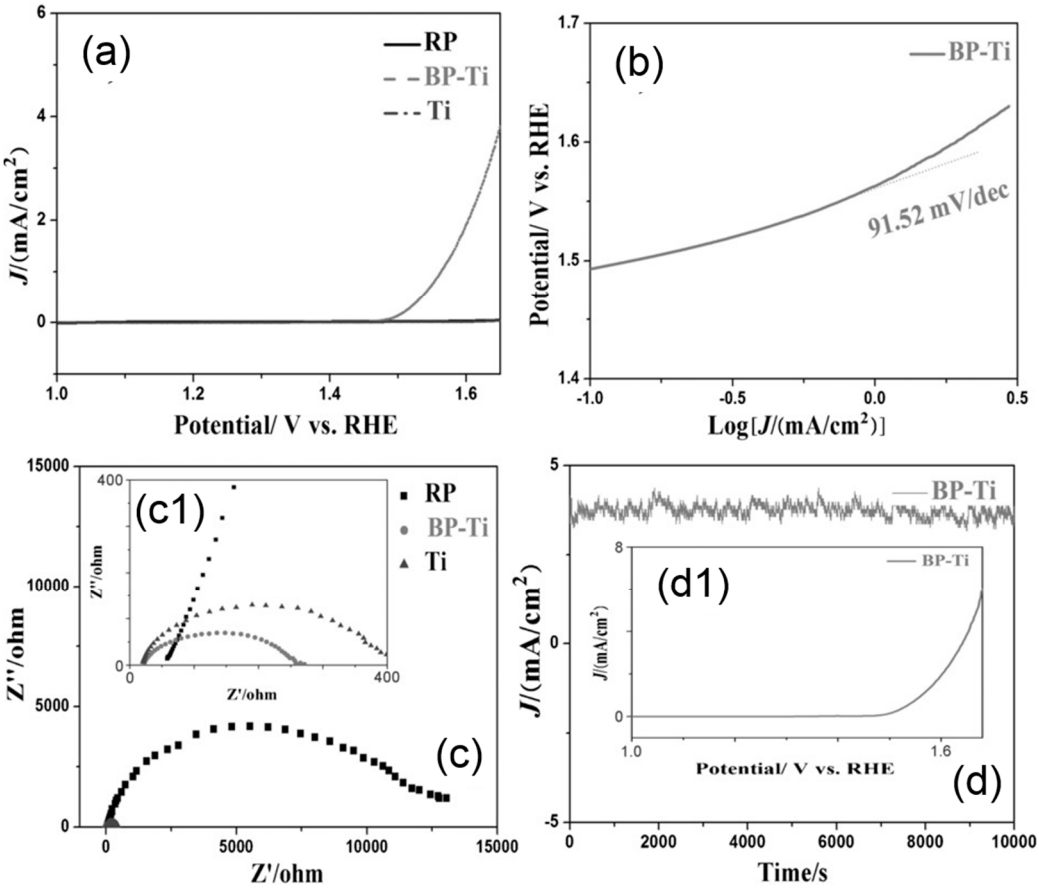

Figure 6. (**a**) Polarization curves of RP, Ti, and BP-Ti in an O_2-saturated potassium hydroxide solution; (**b**) Tafel plots of BP-Ti (**c**) electrochemical impedance spectroscopy (EIS) of RP, BP-Ti, and Ti; (**c1**) the magnified EIS; and, (**d**) chronoamperometric response at 1.65 V (**d1**) polarization curves of BP-Ti before chronoamperometric response. Reprinted with permission from ref. [60]. Copyright 2016 John Wiley and Sons.

Crystalline bulk BP strongly limits the surface area of the catalyst and consequently its performance despite the highlighted intrinsic activity of BP in OER.

A step forward was made by Zhang H. et al. [61], who used exfoliated BP. Following a chemical exfoliation in NMP, a fraction of 2D BP that was made of flakes with a lateral dimension less than 150 nm was isolated and its activity in the OER was tested at different OH^- concentrations. The working electrode was prepared by drop-casting on glassy carbon an alcoholic suspension containing 2D BP that was mixed with carbon black and Nafion. The nanosized 2D BP turned out to be a better electrocatalyst than bulk BP, both in terms of onset potential and current density. In particular, a detailed study was carried out to highlight the effect of nanoflakes thickness. As can be seen in Figure 7a,b the onset potential gets lower increasing the $[OH^-]$, reaching the value of approximately 1.45 V in $[OH^-]$ = 1M. Indeed, while plotting the current density measured at 1.6 V as a function of $[OH^-]$, a linear plot was obtained. Stability tests further revealed how 2D BP nanosheets are promising electrocatalysts for OER. Based on these positive results, subsequent studies have been performed, using BP functionalized with cobalt, either as Co NPs (see Section 5.1) or using the spinel Co_3O_4 [62].

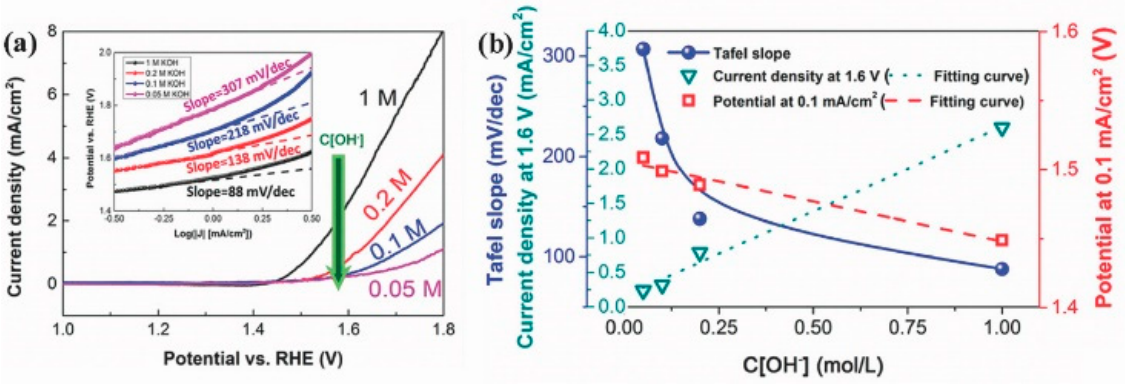

Figure 7. (**a**) Polarization curves and inset corresponding to Tafel plots of BP nanosheets in KOH electrolyte with different concentrations (1, 0.2, 0.1, and 0.05 M). (**b**) Calculated Tafel slope, current density at 1.6 V, and potential at 10 mV cm^{-2} as a function of OH^- concentration. Reprinted with permission from ref. [61]. Copyright 2017 John Wiley and Sons.

4.2. *Electroreduction of N_2 to NH_4^+*

Most of the ammonia worldwide is still produced through the Haber Bosch process, while using harsh reaction conditions and a high energy consumption; thus, many research efforts are addressed to identify the effective catalysts to make ammonia sustainably via nitrogen electroreduction. Common knowledge built up in homogeneous catalysis suggests that, to activate the N≡N triple bond, a transition metal center is needed, which is able to both accept electron density and back donate from its d orbitals toward the π^* orbital of N_2 to weaken the triple bond [63]. This is why the search for nitrogen reduction reaction (NRR) catalysts has mainly focused on transition-metal-based materials. However, recent results have demonstrated that using non-metals as active catalytic sites is feasible [64,65]. Black phosphorus, being a high surface area semiconducting material, which is able to interact with unsaturated systems via weak van der Waals interactions and belonging to the same group of nitrogen, has many promising features. Being aware of that, Wang H. and co-workers [66] studied the application of BP nanosheets (width = 0.5–1.5 μm, thickness ≈4 nm) in NRR. 2D BP turned out to be significantly more efficient than many other published catalysts, both nonmetallic and metal-based ones. A gas-tight two-compartments cell filled with a 0.01 M HCl solution was used in order to perform the NRR, being previously purged and saturated with N_2 (see Figure 8b).

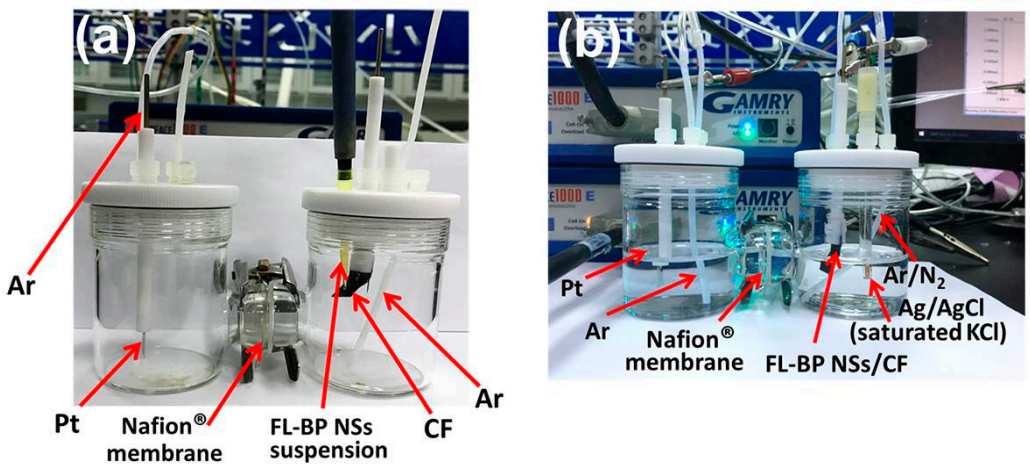

Figure 8. (**a**) The preparation of FL-BP NSs/CF electrode. Few layer black phosphorus nanosheets suspended in ethanol are dropcasted on carbon fiber (CF). (**b**) Reaction cell for NRR. Reprinted with permission from ref. [66]. Copyright 2019 John Wiley and Sons.

The BP nanosheets were supported on carbon fiber that was used as cathode (Figure 8a) and the chronoamperometry curves of electrolysis were recorded over 2 h at different applied potentials, from −0.4 V to −0.8 V vs. RHE under ambient conditions. Figure 9b displays the corresponding measured faradic efficiency. As evident, the maximum faradic efficiency was obtained at a working potential of −0.6 V, while the highest NH_3 yield rate was 31.37 μg h^{-1} mg^{-1}, which was reached at −0.7 V (Figure 9c). Control experiments were also performed to undoubtedly assess the source of ammonia. $^{15}N_2$ was used as feed gas in the cell and, correspondingly, $^{15}NH_4^+$ was detected in solution by ^1H NMR after electrolysis, thus confirming that the feed gas was the only source of nitrogen (Figure 9d). Furthermore, no N_2H_4 (a typical NRR byproduct) was detected in solution. Catalyst durability was also tested, showing how catalytic activity remained almost unaltered after five cycles of chronoamperometric runs (see Figure 9e,f).

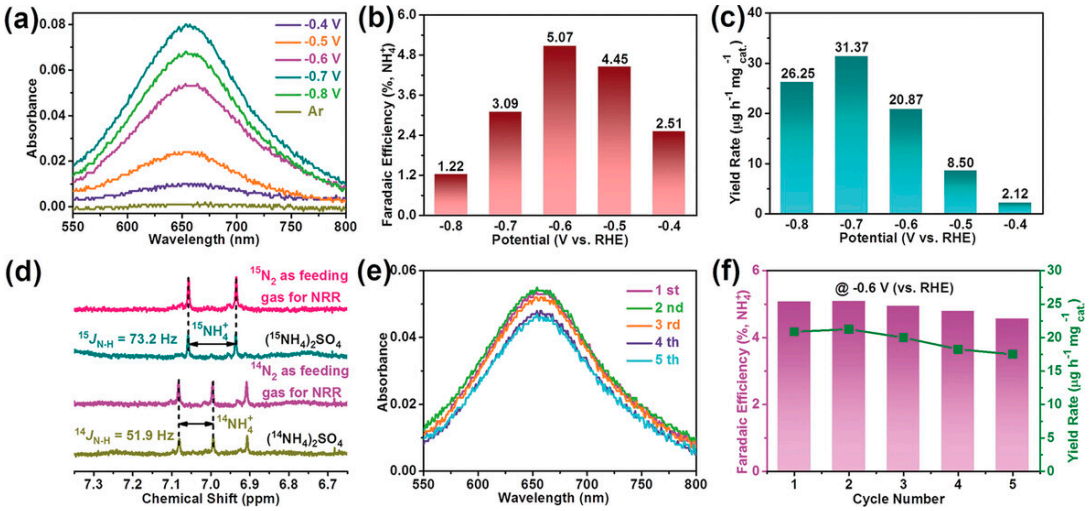

Figure 9. Nitrogen reduction reaction (NRR) behavior of FL-BP NSs/CF. (**a**) Corresponding UV/Vis absorption spectra of the electrolyte (electrolysis at different potentials) stained with indophenol indicator. (**b**) Faradic efficiency and (**c**) NH_3 yield rate at various potentials. (**d**) ^1H NMR spectra (600 MHz) of both $^{14}NH_4^+$ and $^{15}NH_4^+$ produced from the NRR reaction (at −0.6 V vs. RHE) using $^{14}N_2$ or $^{15}N_2$ as the N_2 source. (**e**) Corresponding UV/Vis absorption spectra of the electrolyte (electrolysis on recycled catalyst) stained with indophenol indicator. (**f**) Cycling stability results at −0.6 V (vs. RHE). Reprinted with permission from ref. [66]. Copyright 2019 Wiley.

Theoretical calculations were carried out to identify the nitrogen absorption active sites and clarify the reduction mechanism. As both HOMO and LUMO are more concentrated along edges, denoted as zigzag and diff-zigzag (see Figure 10a,b), these were identified as the active sites for N_2 absorption and reduction.

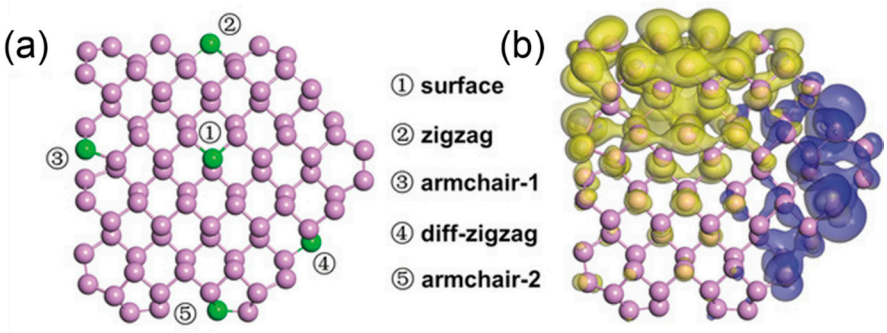

Figure 10. (**a**) Structure of ideal fl-BP NSs (top view). The green balls represent five potential active sites (surface, zigzag, armchair-1, diff-zigzag, and armchair-2 edge). (**b**) LUMO (yellow) and HOMO (blue) of FL-BP NSs. Reprinted with permission from ref. [66]. Copyright 2019 John Wiley and Sons.

These findings prove how elemental substances with an intrinsic Lewis-basic character as BP may be efficiently used for nitrogen fixation under ambient conditions.

4.3. Alkylation of Soft Nucleophiles with Esters

In a seminal publication by G. Abellán and coworkers [67], the feasibility of using 2D black phosphorus and 2D antimonene (2D Sb) to catalyze the alkylation of nucleophiles with esters, even on the gram-scale, has been demonstrated. Alkylation reactions are common steps in organic synthesis, which on both the industrial scale or in laboratories are usually carried out under strong basic or acidic conditions. Alternative catalytic routes, mainly using palladium (i.e., Tsuji-Trost allylation) [68] or copper based catalysts [69], although effective, rely upon toxic or expensive transition metals. The use of 2D pnictogens overcomes all of these problems, which enables a cleaner and functional-group-tolerant protocol to alkylate soft nucleophiles. Black phosphorus nanosheets were prepared exfoliating black phosphorus crystals in ionic liquid (1-butyl-3-methylimidazolium tetrafluoroborate), yielding BP flakes with a lateral dimension of ≈150 nm and an average thickness of 13 nm. A peculiarity of this approach is the use of ionic liquids, both during the preparation of 2D BP and as reaction medium during the catalytic tests. XPS measurements confirmed that the BP surface was efficiently protected by ionic liquids from oxygen and water, largely retarding the degradation, even when directly exposed to air. As a model reaction was selected the alkylation of benzyl alcohol to benzyl *tert*-butyl ether using *tert*-butyl acetate as alkylating agent, as seen in Scheme 2. This reaction might afford two different products, depending on the followed mechanism. As shown in Scheme 1, when cleavage of the alkylic C–O bond in the ester takes place (AL mechanism), the product is benzyl *tert*-butyl ether (the alkylation product), while, if acyl C–O cleavage is operating (AC mechanism), the product is benzyl acetate (acylation product).

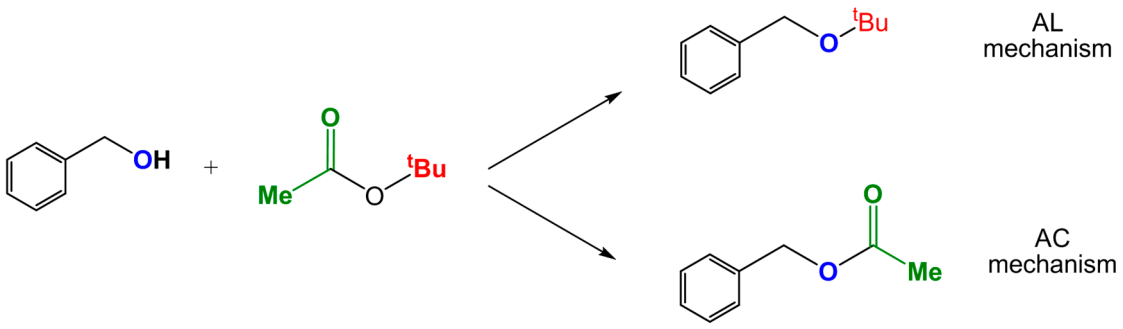

Scheme 2. Two distinct mechanisms are possible, depending on whether the O–C bond in the product involves the alkyl unit (^{t}butyl) or the acyl one (acetyl). The armchair direction (AC) mechanism is more common, i.e., it is the mechanism operating during acid catalyzed trans-esterification. Adapted from ref. [67].

Carrying out the reaction in the presence of 2D BP in ionic liquid, the alkylation product was afforded with extremely high selectivity, >99%, although the yield in the desired product of 46% and the TOF equal 20 h^{-1}. Other 2D materials (for instance graphene) and inorganic acids or bases tested in the same conditions resulted in being catalytically inactive. The only ones giving TOFs that were comparable to 2D BP or 2D-Sb were the strong acids, H_2SO_4 and HOTf, which, however, are not selective, affording a mixture of acylation and alkylation products. A detailed kinetic study was carried out to shed light on the mechanism involving 2D BP (or 2D Sb). The measured kinetic law resulted $v = k_{obs}$ (alcohol)(ester)(2D BP), which indicated that the three species, i.e., the nucleophile, the ester, and BP, are involved in the rate limiting step. When strong acid catalysts are used, alkylations go through carbocationic intermediates (in this case ^{t}Bu$^+$), which are trapped by the nucleophile. The authors showed that this occurs also when 2D-pnictogens are used as catalysts. A parallel experiment was devised using a chiral ester to alkylate methanol, affording a racemic mixture of the alkylated product, to highlight the presence of such carbocationic intermediate (see Scheme 3).

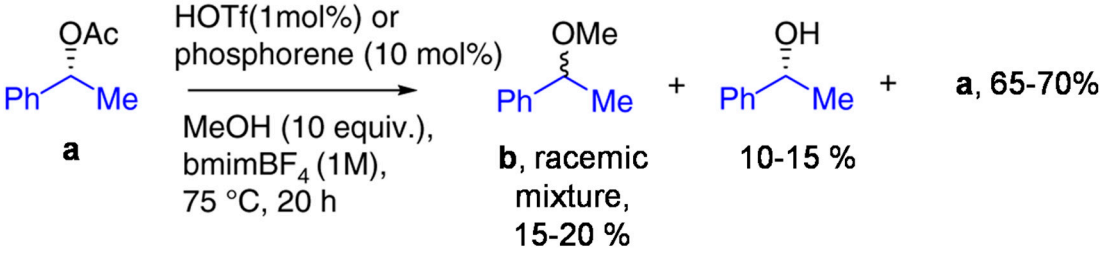

Scheme 3. Experimental evidence for the presence of a carbocationic intermediate. Starting from enantiomerically pure **a**, the alkylated product **b** is obtained as a raceme both with 2D BP or with HOTf as catalyst. Adapted from ref. [67].

Based on these findings, alongside further studies, the authors proposed the mechanism that is displayed in Figure 11 for the catalyzed alkylation of benzylic alcohol with esters.

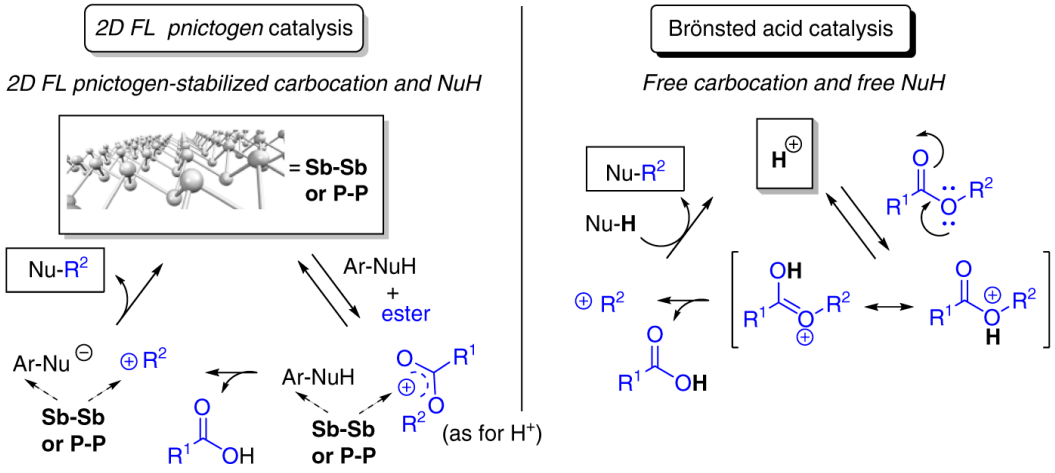

Figure 11. Proposed reaction mechanism for the 2D BP (2D Sb)-catalyzed alkylation of nucleophiles with esters (left) compared with the classic strong-acid-catalyzed mechanism (right). Adapted from ref. [61].

Benzylic alcohol is easily adsorbed on the surface of black phosphorus. Such non-covalent interaction between 2D BP and unsaturated rings is well known [34,52]. The 2D BP surface acts as an electron donor towards the adsorbed aromatic nucleophile, and this donation generates a deficiency of charge on 2D BP, which activates the ester group (somehow 2D BP would take the role of the acidic proton in the strong-acid-catalyzed mechanism), stabilizing the carboxonium ion and the carbocation that were formed by the oxonium/carbocation equilibrium. Once formed, the stabilized carbocation would then be trapped by the adsorbed nucleophile, ending a catalytic cycle and regenerating the electroneutrality of the surface.

5. Metal Nanoparticles Decorated Black Phosphorus

As discussed above, the intrinsic properties of black phosphorus allow for its application in catalysis as a pristine material, while the feasibility of its surface functionalization gives the opportunity to broaden its scope. In this respect, the coordinative abilities of black phosphorus render it particularly suitable to anchor metal nanoparticles. Usually, the physical and chemical properties of the modified material are not just a sum of those of the individual constituents. The mutual interaction between the metal nanoparticles and the 2D BP surface imparts an entirely new reactivity to the heterostructure. This can depend on the energetics of the metal-phosphorus interface, as in the case of Co NPs/BP (see Section 5.1), or it can be the result of some ancillary role played by 2D BP orienting the selectivity toward a specific product during a catalytic cycle, as in the case of Pd NPs-modified BP (see Section 5.3).

5.1. Cobalt

Cobalt nanoparticles were immobilized on black phosphorus nanosheets via a one-pot solvothermal reduction [70], heating a BP suspension in the presence of $Co(OAc)_2 \cdot 4H_2O$ in oleylamine at 245 °C for 1 h. The oleylamine served as both a solvent and as reducing agent toward Co^{2+}. XRD and HRTEM analysis confirmed the presence of nanometric f_{cc} Co domains (≈21 nm) that were supported on the surface of black phosphorus, thus assessing the formation of a Co/BP nanohybrid (Figure 12).

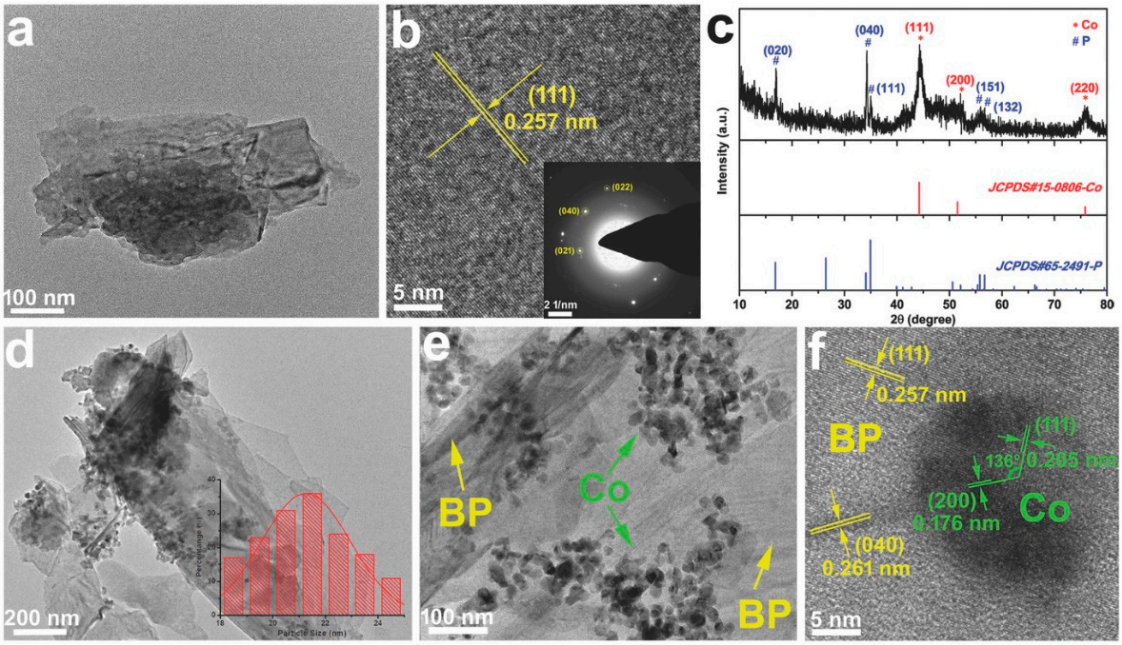

Figure 12. (**a**) XRD patterns of the as-prepared Co/BP nanohybrids. (**b**) TEM image of the exfoliated BP nanosheets with the size of hundreds of nanometers. (**c**) HRTEM image of the BP nanosheets (the insets are corresponding SAED patterns). (**d**,**e**) TEM images of the Co/BP. (**f**) HRTEM image of the Co/BP. Reproduced from ref. [70].

The P 2p XPS spectrum of the nanohybrid showed a blue shift in all the peaks ($P2p_{1/2}$, $P2p_{3/2}$, and P–O) when compared to pristine black phosphorus. This increase in binding energy was complemented by the red shift observed for the Co (0) peaks as compared to bare Co NPs, thus experimentally revealing electron migration from BP to Co through the Co/BP interface, as rationalized when considering the higher Fermi level of BP than of metallic cobalt (Figure 13).

Performances in the oxygen evolution reaction (OER) were evaluated by linear sweep voltammetry (LSV) while using pristine BP, Co NPs, and commercial IrO_2 for comparison to evaluate the electrocatalytic activity of the new Co/BP nanohybrid. While both BP and Co NPs individually resulted poorly effective in OER, Co/BP performed exceptionally with the same onset potential of ≈210 mV as commercial IrO_2, and even outperforming it in activity above the overpotential of 310 mV (Figure 14). Interestingly, a physical mixture of Co NPs and BP, although able to catalyze the OER, resulted in being much less active than the nanohybrid Co/BP, thus highlighting the role that is played by the Co/BP interface and the importance of directly growing the Co NPs on BP. Interestingly, Co/bP also demonstrated excellent stability in alkaline media, suggesting that it could be, in principle, a potential alternative to the expensive IrO_2.

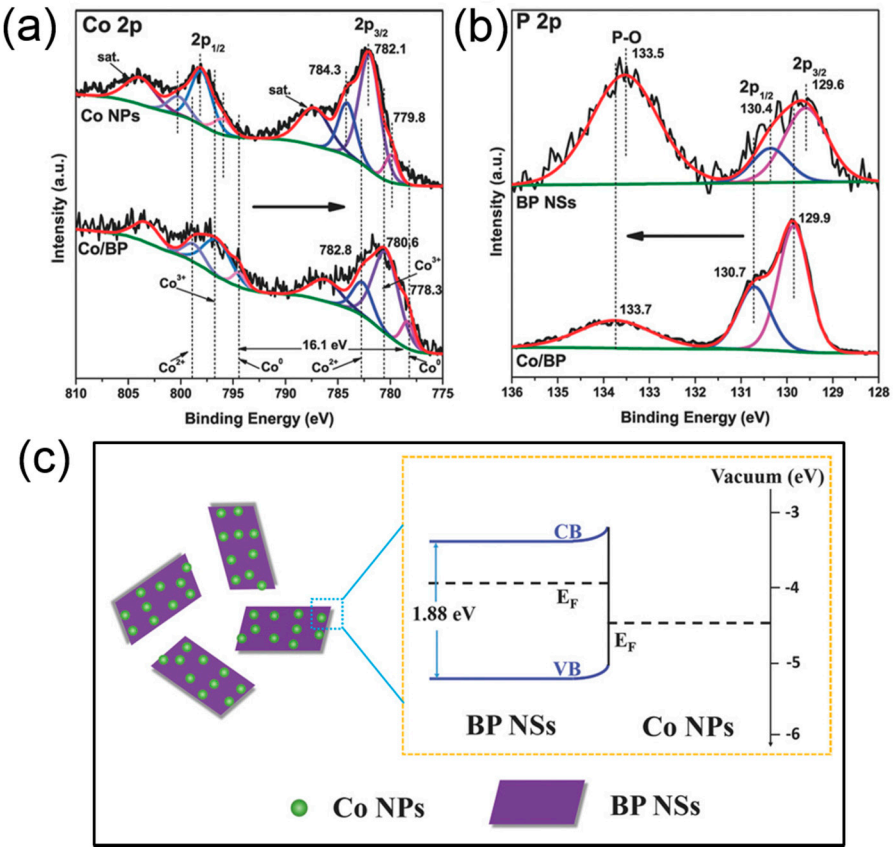

Figure 13. (**a**) Co 2p XPS core level spectrum of Co/BP and bare Co NPs. There is a shift of ≈1.5 eV for Co in Co/BP toward lower BE. (**b**) P 2p XPS core level spectrum of Co/BP and pristine BP. The peaks in Co/BP are slightly shifted toward higher energy. (**c**) Energy band diagram for the Co/BP nanohybrid. Reproduced from ref. [70].

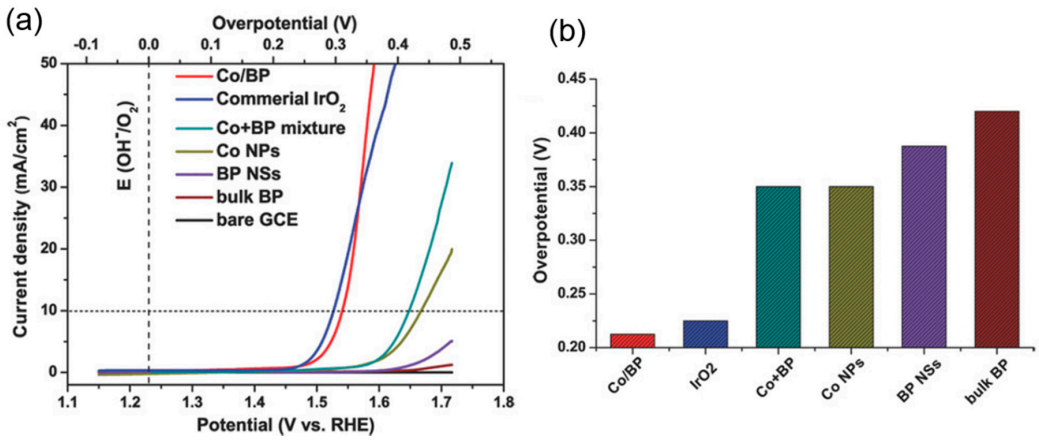

Figure 14. (**a**) Linear sweep voltammetry (LSV) curves and (**b**) onset overpotential of Co/BP nanohybrids, commercial IrO_2, the physical mixture of Co + BP, Co NPs, BP NSs, the bulk BP, and bare glassy carbon electrode (GCE). Reproduced from ref. [70].

5.2. Nickel

One of the first successful decorations of black phosphorus with metal nanoparticles was the one with Ni that was reported by us [36]. We immobilized preformed Ni NPs on exfoliated BP via the simple addition of colloidal Ni NPs (≈12 nm) to a BP suspension. Exfoliated black phosphorus

resulted in being capable of stabilizing Ni NPs on its surface, even to a very high molar ratio P/Ni = 3, and the morphology of the nanohybrid was studied by TEM and HR TEM (Figure 15a,b).

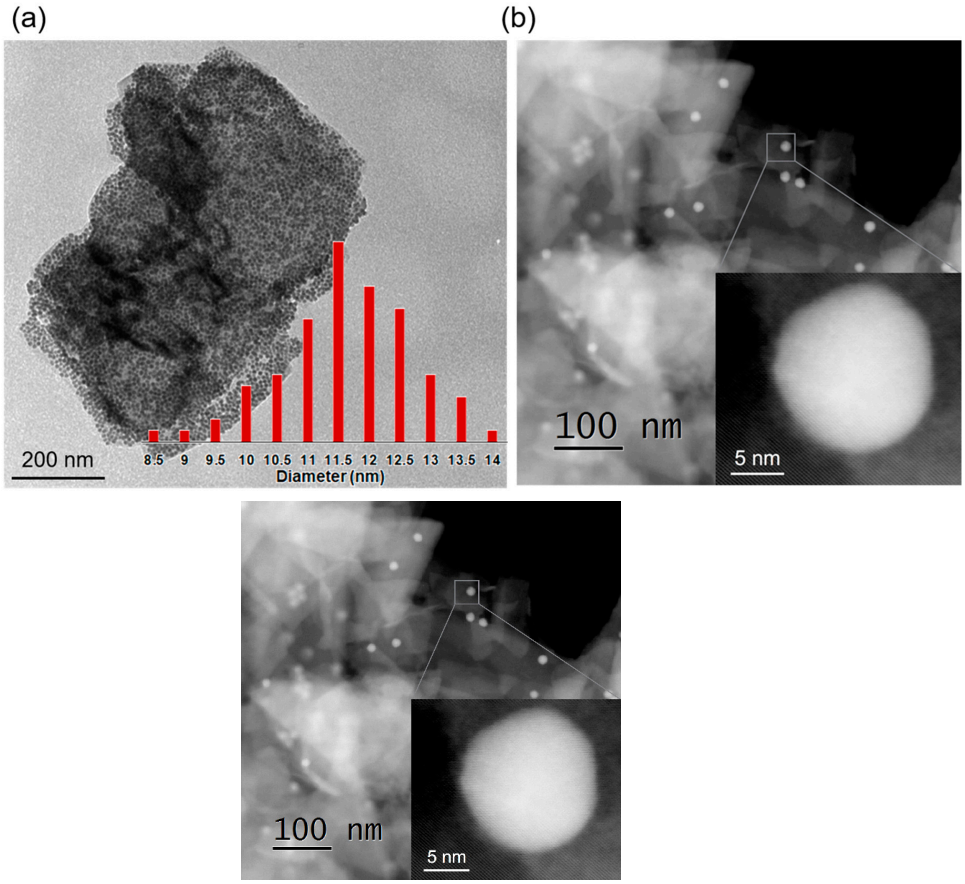

Figure 15. (**a**) TEM image of Ni NPs supported on few-layer black phosphorus (Scale bar: 200 nm), P:Ni molar ratio 3:1, and corresponding size distribution. (**b**) HR TEM image of Ni/2D BP. Adapted from ref. [36] Copyright 2017 The Authors.

The environmental stability test showed that the Ni-functionalized material was much more stable than pristine BP, remaining morphologically unaltered after one week of air exposure. The ability of BP to stabilize Ni NPs on its surface was exploited while using the nanohybrid as a catalyst for the selective hydrogenation of phenylacetylene (PA) to styrene. This catalytic conversion is of practical interest in the petrochemical industry, polymerization industry, and manufacture of pharmaceuticals [71]. For instance, with PA being present in styrene feedstock as an impurity, it can deactivate polymerization catalysts, so its removal is mandatory. However, many hydrogenation catalysts are unable to stop at the semi-hydrogenation level and further reduce styrene to ethylbenzene. Heterogeneous catalysts that are based on noble metals, such as Pd, Pt, and Au, are usually used in this process, thus the search for abundant and low-cost metals is highly desirable [72]. Ni/BP turned out to be very selective, affording 92.8% of styrene at quantitative conversion, when compared to 78.6% of bare Ni NPs. The recycling test also showed the reusability of the catalyst, while bare Ni NPs were deactivated after the first catalytic run (see Figure 16). Known heterogeneous catalysts that are based on supported nickel metal, as Ni/Al_2O_3 [73], Ni/MgO [74], and Ni@C [75] have shown in this reaction much lower chemoselectivity, 0.7%, 36.0%, and 60%, respectively, thus the important role of 2D bP as support is emerging.

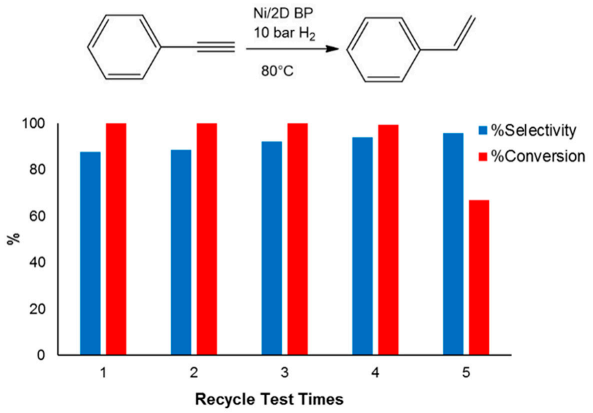

Figure 16. Recycling tests. Reaction conditions: 10 bar H_2, 80 °C, 2 h, Ni NPs = 1.2 mol %, phenylacetylene = 0.3 mmol, 1.41 mg catalyst (15.2 wt % Ni). Reproduced from ref. [36] Copyright 2017 The Authors.

5.3. Palladium

Small Pd NPs (≈3.2 nm) were grown on exfoliated black phosphorus by us [76] via an in situ reduction while using molecular hydrogen as reductant, the structural characterization of the resulting nanohybrid Pd/BP is shown in Figure 17.

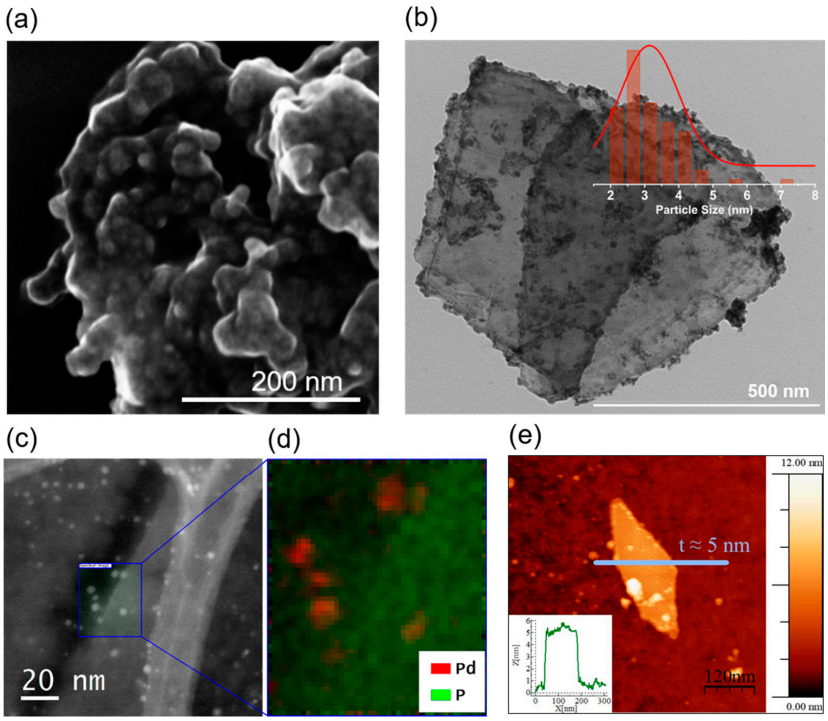

Figure 17. (**a**) SEM image of Pd/BP. (**b**) Transmission electron microscopy (TEM) image of Pd/BP and relative size distribution. (**c**) High-resolution HAADF STEM (High-Angle Annular Dark-Field Scanning Transmission Electron Microscopy) image of Pd/BP on a lacey carbon grid. Pd-rich areas can be clearly distinguished for the higher Z-contrast (brighter areas). The blue region of interest indicates the region in which the EDS (Energy-dispersive X-ray spectroscopy) SI (spectrum imaging) was performed. (**d**) EDS elemental mapping of the selected area on Pd/BP obtained by integrating the signals from the Pd L-lines and the P K-lines. (**e**) AFM image of a Pd/BP flake on Si/SiO_2. The line corresponds to the cross-sectional profile shown as an inset. The flake thickness is approximately 5 nm. Reproduced from ref. [76] Copyright 2019 American Chemical Society.

XPS and XRD revealed that the NPs that were anchored on the BP flakes corresponded to an f_{cc} Pd phase. The nature of the interaction between Pd and black phosphorus was deeply investigated. EELS measurement at the P_k edge revealed a modification in the spectrum profile when compared to pristine BP, which was attributed to a modification of the electronic structure of phosphorus. Pd 3d XPS measurement further corroborated these findings, which revealed a double contribution to the Pd $3d_{3/2}$ and $3d_{5/2}$ peaks (Figure 18).

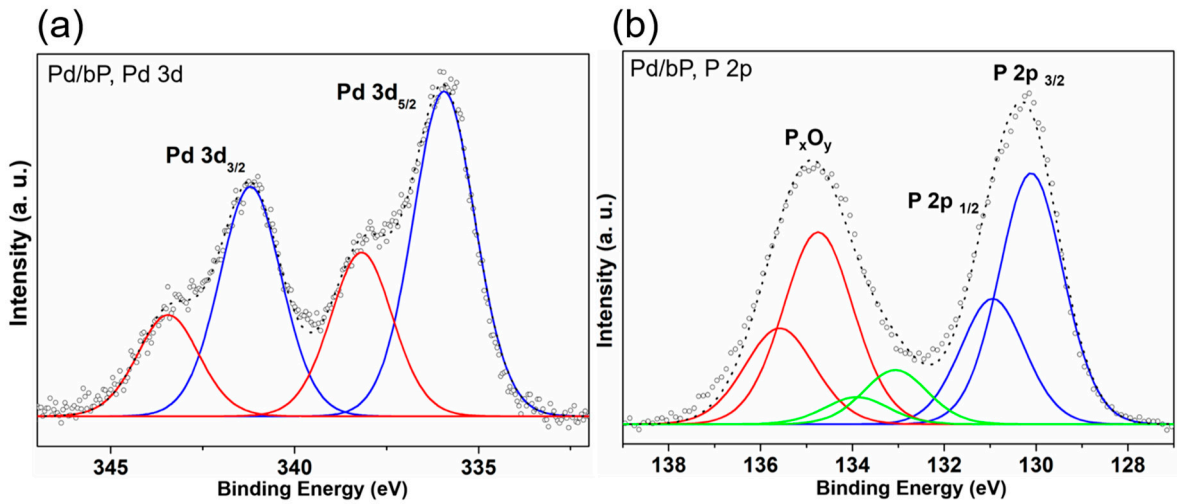

Figure 18. (**a**) Pd 3d and P 2p (**b**) XPS core level spectrum of Pd/BP. Reproduced from ref. [76] Copyright 2019 American Chemical Society.

One is located at the typical binding energy of metallic palladium and it corresponds to the Pd NPs core. The other, which shifted at higher binding energies, results from the outer Pd atoms of the nanoparticles that are involved in Pd–P bonds. Such spectral feature is typical of Pd NPs that are capped with molecular phosphorus ligands strongly interacting with the metal surface. Indeed, EXAFS (Extended X-ray Absorption Fine Structure) measurement revealed a surprisingly short Pd–P distance of 2.26 Å, inferring the presence of a covalent bond. The ability of black phosphorus to strongly bind Pd NPs and the high catalytic activity of metallic Pd in hydrogenation reactions, suggested the application of this nanohybrid in the selective hydrogenation of chloronitroarenes to chloroanilines. The transformation of nitroarenes into the corresponding anilines is one of the most important manufacturing processes, since amino compounds are intermediates in the synthesis of pharmaceuticals, agrochemicals, pesticides, and organic dyes [77]. Secondly, it is well known that nitrocompounds, being toxic and carcinogenic, are pollutants and dangerous for the environment and living organisms, thus their removal is mandatory [78]. Many different methods have been developed to attain a highly selective reaction, for instance, a straight catalytic conversion of chloronitroarenes to haloanilines is usually affected by the undesired dehalogenation reaction, which affords simple aniline as byproduct (see Figure 19a). Remarkably, Pd/BP performed the reduction with a selectivity as high as 99.7% at 99.5% conversion, which is superior to other heterogeneous 2D catalysts that are based on supported Pd NPs [79]. Pd NPs supported on carbon also resulted in being much less selective (78.1%), showing how the synergy between black phosphorus and palladium is crucial for attaining high selectivity. Catalyst recycling tests also highlighted the durability of the catalytic system, which kept its activity and selectivity almost unaltered for five consecutive runs (see Figure 19b). The observed selectivity may be explained considering the preferential interaction of BP with the more electron-poor chloronitrobenzene with respect to chloroaniline, favoring the displacement of the latter from the BP surface after the NO_2-group reduction has taken place, thus avoiding the additional hydrogenation of the C–Cl bond in chloroaniline once formed.

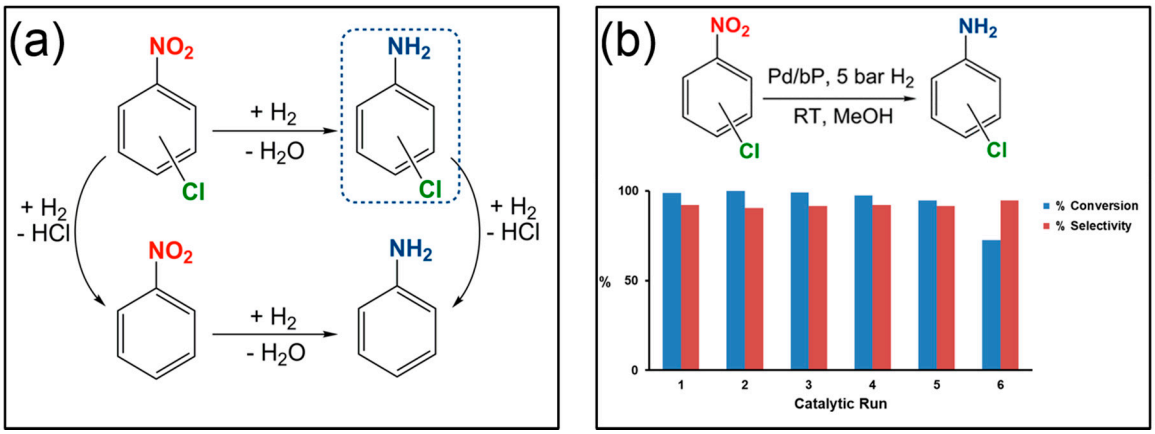

Figure 19. (**a**) The two possible pathways for the secondary reaction of C–Cl hydrogenolysis. (**b**) Catalyst reuse in the hydrogenation of 1-chloro-2-nitrobenzene. Reproduced from ref. [76] Copyright 2019 American Chemical Society.

Other fields have been triggered next to the application of Pd/BP in a purely chemical process as the hydrogenation of organic substrates, in particular the one of fuel cells that represents a milestone in the development of green energy resources aiming to solve the problem of the fast consumption of limited fossil fuels. Direct ethanol fuel cells (DEFCs) are recognized as being of good promise, since ethanol is a plentiful and low cost liquid fuel that can be prepared by the biomass. Min Y. et al. [80] exploited the efficiency of Pd in the ethanol oxidation reaction (EOR) and some features of previously reported Pd/TiO_2 electrocatalysts to devise a catalyst made of Pd NPs supported on a hybrid anatase TiO_2 nanosheets (ATN)-black phosphorus support, where the latter has the role of compensating the low conductivity of ATN. Additionally, BP was chosen, since it can serve as excellent sites for water dissociative adsorption accelerating the formation of OH radicals that react with CH_3CO radicals on the Pd active site to generate the product of ethanol oxidation, i.e., acetate ions. The ATN-BP hybrid was prepared by prolonged ball milling of BP nanosheets and ATN, which promotes an intimate mixing of the two materials. Careful experimental studies were carried out in order to clarify the degree to which the two materials were mixed. The main XRD peaks of TiO_2 were still visible after ball milling, which suggested the retention of its crystalline structure. On the other hand, the BP lattice resulted in being mainly disrupted, as confirmed by the P 2p XPS spectrum, where a large P–O peak was visible, the oxygen coming from the ATN phase. O 1s XPS remarkably showed a characteristic peak due to P–O–Ti units, thus revealing the oxo-linkage between BP and ATN domains (See Figure 20a). This hybrid support was decorated with palladium while using the wet reduction process, obtaining Pd NPs (≈10.2 nm) that were mainly localized along the edge of the ATN-BP support. Pd 3d XPS measurements highlighted the simultaneous presence of different valence states that were assigned to Pd (0), PdO_x, and Pd_3Ti (Figure 20b).

Cyclic voltammetry investigated the electrocatalytic performance of Pd/ATN-BP in the EOR in a solution 1.0 M in both NaOH and EtOH. Remarkably, the mass peak current density was much higher than commercial Pd/C, Pd/ATN, Pd/BP, and of many other previously reported EOR Pd-catalysts. Furthermore, Pd/ATN-BP displayed excellent catalyst durability when compared to the other reference catalysts. Thus, the structure of ATN-BP resulted in being beneficial for improving the electrolyte penetration and the electron transport, but it also played a beneficial influence on the stripping of reactive intermediates as CO_{ads} that would otherwise poison the catalyst.

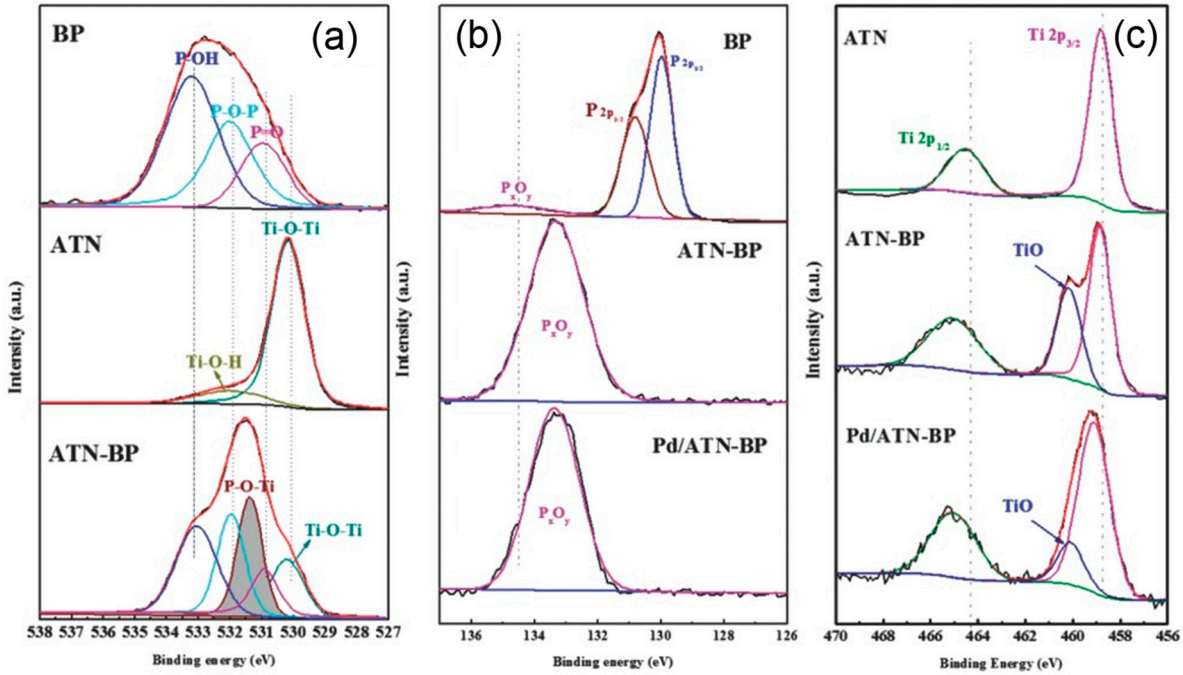

Figure 20. (**a**) Deconvolution of the O 1s XPS spectra of BP, anatase TiO_2 nanosheets (ATN), and ATN-BP. (**b**) Deconvolution of the P 2p XPS spectra of BP, ATN-BP, and Pd/ATN-BP. (**c**) Fitted high-resolution Ti 2p spectra of ATN, ATN-BP, and Pd/ATN-BP. Reprinted with permission from ref. [80]. Copyright 2017 Wiley-VCH Verlag GmbH & Co.

A follow-up of this work came one year later by the same group who supported palladium nanoparticles on a black phosphorus-graphene heterostructure [81]. Through merely ball-milling of activated graphene (AG) and BP, a new heterostructure AG-BP was obtained, where the sheets are covalently connected by P-C bonds (see Figure 21).

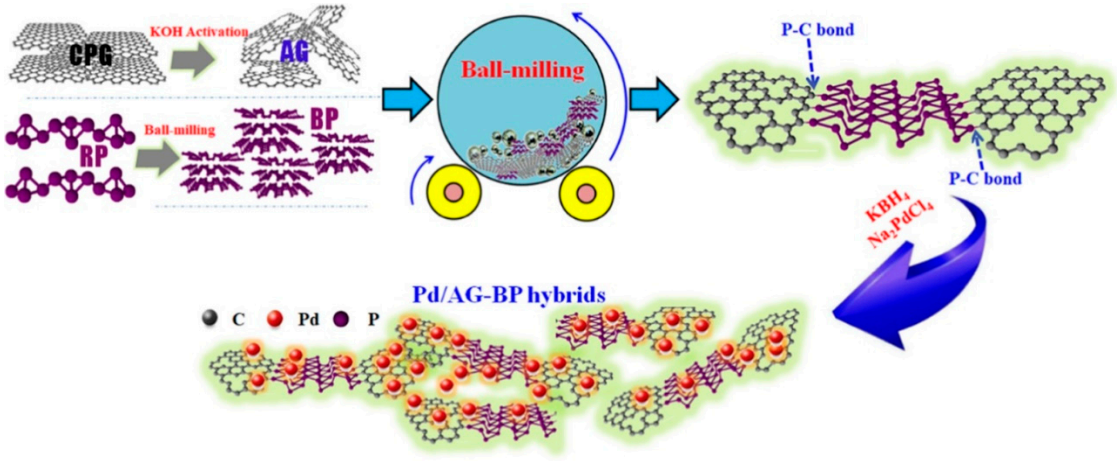

Figure 21. Schematic diagram for the preparation of Pd/AG–BP catalysts. Reprinted with permission from ref. [81]. Copyright 2019 American Chemical Society.

The electron transfer from Pd NPs (grown on the heterostructure) to AG-BP creates a positive charge on Pd that is more prone to absorb OH radicals that combine with CO_{ads} intermediate releasing active sites for EOR process, according to experimental and DFT studies. The obtained Pd/AG-BP hybrid exhibited higher electrochemical activity than the previously reported Pd/ATN-BP.

5.4. Platinum

Xue-Feng Yu et al. succeeded in functionalizing 2D BP flakes with ultrasmall platinum nanoparticles (≈1.1 nm) while using an in situ reduction process [82]. The novel Pt/BP heterostructure showed greater environmental stability when compared to pristine black phosphorus, keeping its morphology almost intact for at least 15 days of air exposure. XPS measurements studied the composition of the surface. The Pt 4f XPS spectrum displayed the two spin-orbit components ($4f_{7/2}$ and $4f_{5/2}$), each one further split. One component, which corresponded to metallic Pt, was attributed to the NP's core. The other is shifted at higher binding energy, suggesting the formation of a surface Pt-P bond. As a confirmation, this higher energy component is absent in the XPS spectrum of Pt nanoparticles that were supported on P25 (TiO_2) or SiO_2 (see Figure 22a) As the O 1s spectrum of Pt/BP, besides the native P_xO_y peaks at 532.7 and 531.4 eV, displays a new smaller peak at 530.5 eV; this spectral feature was taken as an indication of some Pt–O bond (Figure 22b).

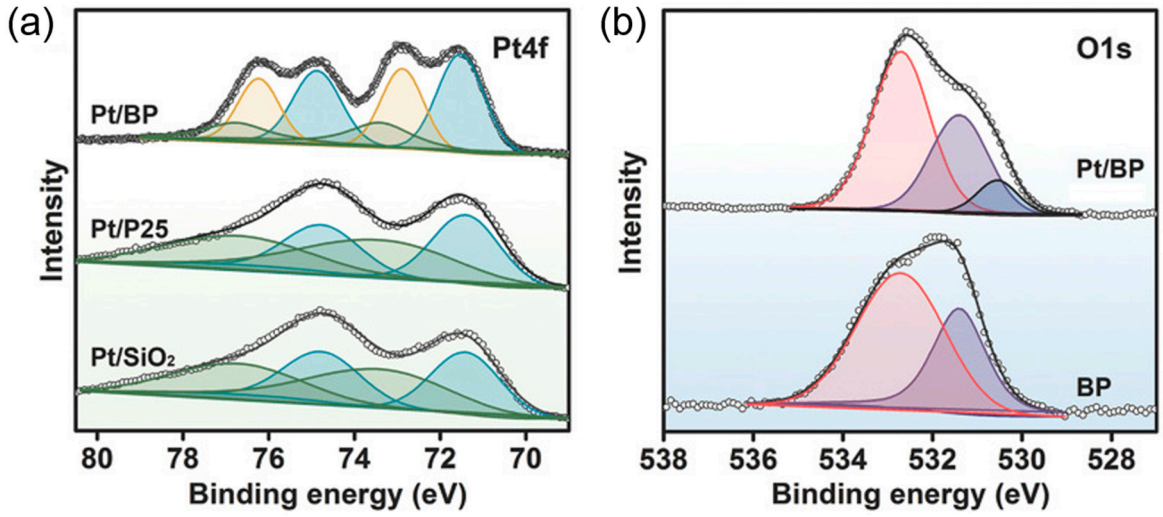

Figure 22. (**a**) Pt 4f core level XPS of Pt/BP, Pt/P25(TiO_2), and Pt/SiO_2. The blue peaks corresponds to Pt (0) from the NP's core. The other two components are due to Pt-P (yellow) and Pt_xO_y (green). (**b**) O 1s core level XPS of Pt/BP and pristine BP. The extra peak at 530.5 eV is due to Pt–O bonds. Reproduced from ref. [82]. Copyright 2018 John Wiley and Sons.

It was possible to show how photogenerated electrons promoted to the conduction band of BP were transferred to the Pt NPs, producing a slight shift in the Pt 4f levels toward lower energies, by means of in situ XPS measurements that were performed while illuminating the heterostructure with green laser light. Such an ability of the Pt centers to accumulate negative charge was exploited while using the Pt/BP heterostructure to promote electron-assisted photochemical reactions. Styrene was hydrogenated to ethylbenzene under solar light simulated irradiation as a benchmark catalytic test, and the performances of Pt/BP were compared with other Pt-based catalysts. Pt/BP showed excellent photocatalytic activity, being much higher than commercial Pt/C or Pt NPs that were immobilized on SiO_2 or TiO_2 (see Figure 23a).

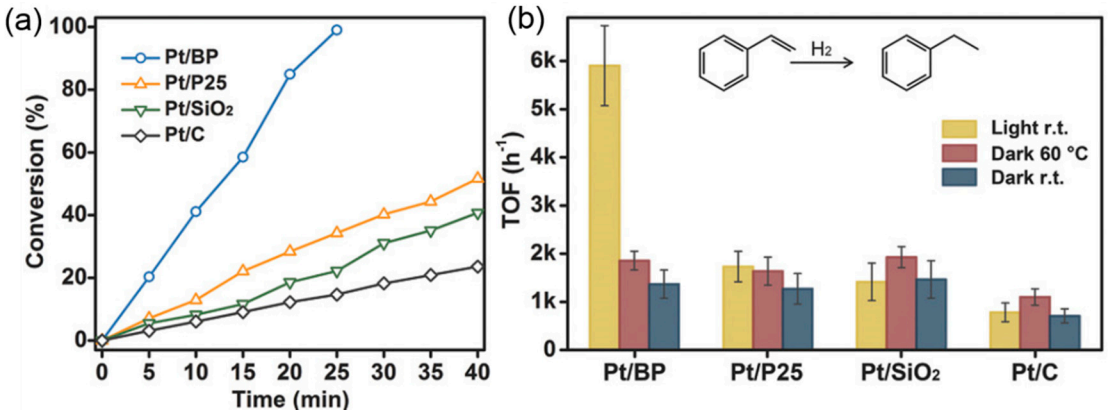

Figure 23. (**a**) Conversion/time plots under simulated solar light illuminations (styrene/Pt = 24.3) (**b**) Catalytic performance obtained for the various Pt catalysts under different illumination and thermal conditions. Reprinted with permission from ref. [82]. Copyright © 2020 John Wiley and Sons.

Moreover, carrying out the reaction in the dark, the measured TOF dropped to the value of the other catalysts, which were mainly unaffected by light irradiation conditions. Pt NPs that were immobilized on P25 (TiO_2) showed an increase in TOF of ≈36% under light irradiation, being much lower than the increase of 400% that was exhibited by Pt/BP (Figure 23b).

A completely different approach was adopted by the same authors studying the rather surprising ability of black phosphorus to act like a surface dopant activating preformed Pt NPs (~3 nm) toward HER reaction [83]. The authors investigated how Pt NPs that were supported on different carbonaceous support may undergo lattice distortion, incorporating P atoms in their outer shell when treated in ethanol with exfoliated BP under ultrasounds, both theoretically and experimentally. XRD recorded before and after treatment with black phosphorus highlighted lattice opening and the incorporation of phosphorus in the f_{cc} metallic phase of platinum, as the characteristic (111) and (200) peaks of metallic Pt almost disappeared (Figure 24). HRTEM also observed a significant loss of crystallinity. Correspondingly, Pt 4f XPS spectra showed the appearance of a Pt (II) peak assigned to Pt–P bonds. Despite that there is no mention of a platinum phosphide phase in the paper, it seems reasonable to view the process as the growth of an amorphous metal-rich Pt_xP phase.

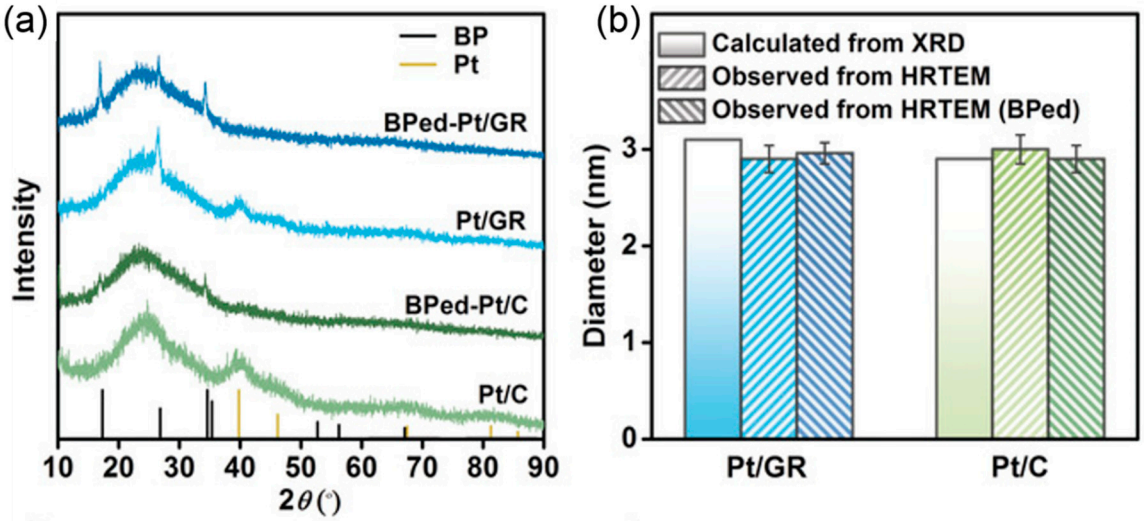

Figure 24. (**a**) XRD spectra of Pt on graphite (Pt/GR), BP-treated Pt on graphite (BPed-Pt/GR), commercial Pt/C and BP-treated commercial Pt/C (BPed-Pt/C). (**b**) Measured Pt NPs dimensions before and after treatment with BP. Reprinted with permission from ref. [83]. Copyright © 2020 John Wiley and Sons.

Being known that platinum is an excellent cocatalyst for the hydrogen production, because it can reduce the overpotential of hydrogen evolution from water, the resulting nanocomposite was evaluated as the catalyst in the HER reaction in alkaline medium. Different Pt-P bonds content (as determined by integration of the XPS peaks) was tested over a range between 0% (no BP treatment) and 45%, as the amount of phosphorus incorporated could be controlled by varying the volume of BP nanosheets suspension added during the synthesis, with the best performance obtained using the sample with 21% Pt–P (see Figure 25). Notably, not only the activity of simple Pt NPs could be improved, but many state-of-the-art Pt based catalysts were overcome.

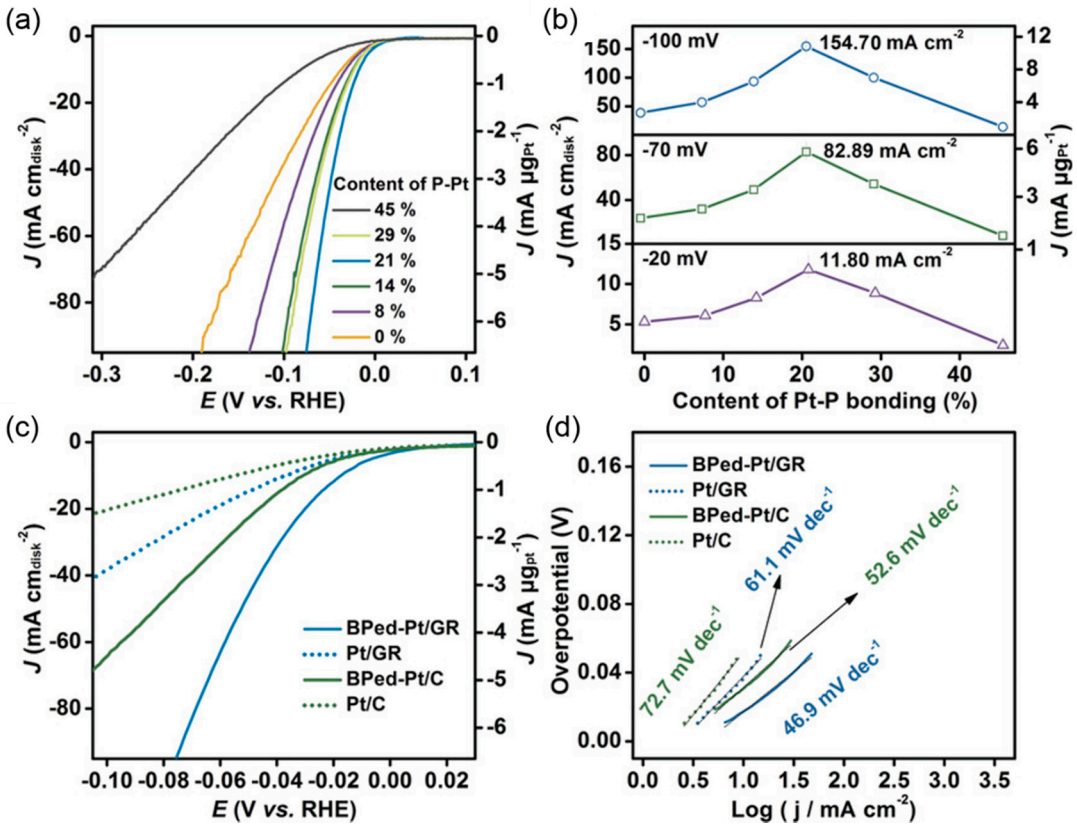

Figure 25. Catalytic performances of Pt NPs supported on carbon supports, with and without previous activation with black phosphorus. (**a**) Hydrogen evolution reaction (HER) polarization curves of BPed-Pt/GR with different content of Pt-P bonds in 1 M KOH at 25 °C. (**b**) Current densities of BPed-Pt/GR with Pt–P content of 21%, 14% and 8% (from top to down) at 100, 70 and 20 mV vs RHE. (**c**) HER polarization curves of BPed-Pt/GR (21%), Pt/GR, BPed-Pt/C (23%), and Pt/C in 1 M KOH at 25 °C. (**d**) Corresponding Tafel slope values for each curve in (**c**). Reprinted with permission from ref. [83]. Copyright © 2020 John Wiley and Sons.

Following this encouraging results, another contribution to the study of HER comes from the group of Liu Y., [84], who firstly found a new way to prepare BP nanosheets while using a solvothermal bottom-up procedure, based on heating white phosphorus in ethylendiamine at 140 °C overnight. The obtained BP nanosheets resulted in being partially oxidized, although they performed efficiently in the reaction of hydrogen evolution, which was conducted in pure water under irradiation in the Vis-NIR region, without adding sacrificial agents. Metal-free BP exhibited an activity more than 24-fold times higher of the well-known C_3N_4 nanosheets, as shown in Figure 26. An additional increase of catalytic activity was observed once BP was functionalized with 20 wt % PtNPs.

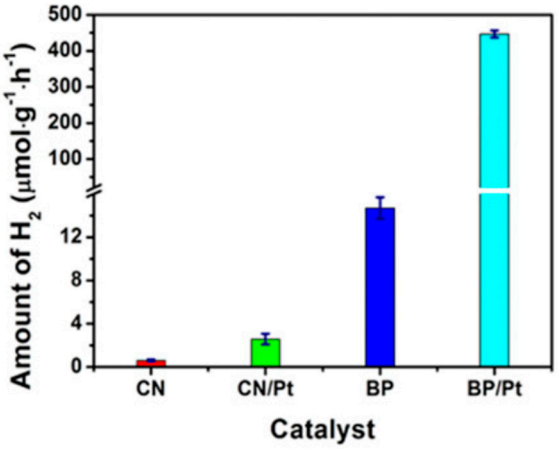

Figure 26. Hydrogen evolution rates from pure water (pH = 6.8) using BP and 20 wt % Pt/BP as catalysts under irradiation of a 300-W Xe lamp (PLS-SXE300C, $\lambda \geq 420$ nm). For a comparison, hydrogen evolution rates using C_3N_4, pristine BP, 1 wt % Pt supported on C_3N_4 were also measured. Adapted from Ref. [84].

5.5. Silver

Silver nanoparticles were grown on 2D BP nanosheets by reducing $AgNO_3$ with $NaBH_4$ in a water solution [85]. Two different metal loadings were used, 3 and 5 wt %, with average Ag NPs dimensions of 20 and 40 nm, respectively (see Figure 27).

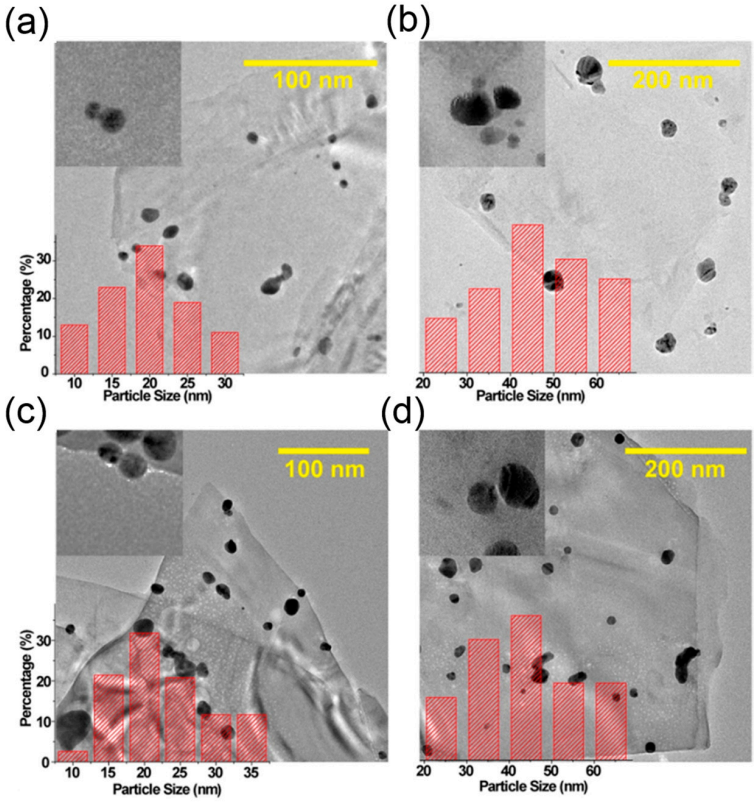

Figure 27. TEM images of Ag/2D BP. (**a**) 3 wt % Ag/f-BP (few layer BP, ~4 layers thickness. (**b**) 5 wt % Ag/f-BP (**c**) 3 wt % Ag/m-BP (multilayer BP, ~20 layers thickness). (**d**) 5 wt % Ag/m-BP. Reprinted with permission from ref. [85]. Copyright © 2020 American Chemical Society.

DFT studied the interaction between silver and black phosphorus; Ag adlayers stacked above a slub of black phosphorus was chosen as a simplified system. The calculations showed how the growth of Ag NPs on 2D BP is driven by the formation of the new Ag–Ag interaction more than Ag–P bonds. Indeed, moving from 0.25 monolayers of Ag coverage to two monolayers, the adsorption energy decreases, while the Ag–P bond distances increases, going from a scenario that was characterized by an ionic interaction to one better described in terms of a covalent interaction between Ag and P. The performance of the new Ag/2D BP nanohybrid in the photocatalytic degradation of rhodamine B (RhB) in water, a model reaction of environmental purification, was then investigated. The photoactivity of Ag/2D BP turned out to be layer dependent, increasing with decreasing 2D BP layer thickness (see Figure 27). Increasing the Ag loading, there was a parallel enhancement of RhB degradation. These findings were explained while carrying out photocurrent measurements. The experimental set-up adopted was a typical three electrode cell, where Ag/2D BP had been dropcasted on the working electrode and the solution was then subjected to on-off illumination from a xenon lamp during the measurements. The results, as reported in Figure 28, clearly reproduce the trend previously described, with higher current densities being favored by thinner flakes and higher metal loadings.

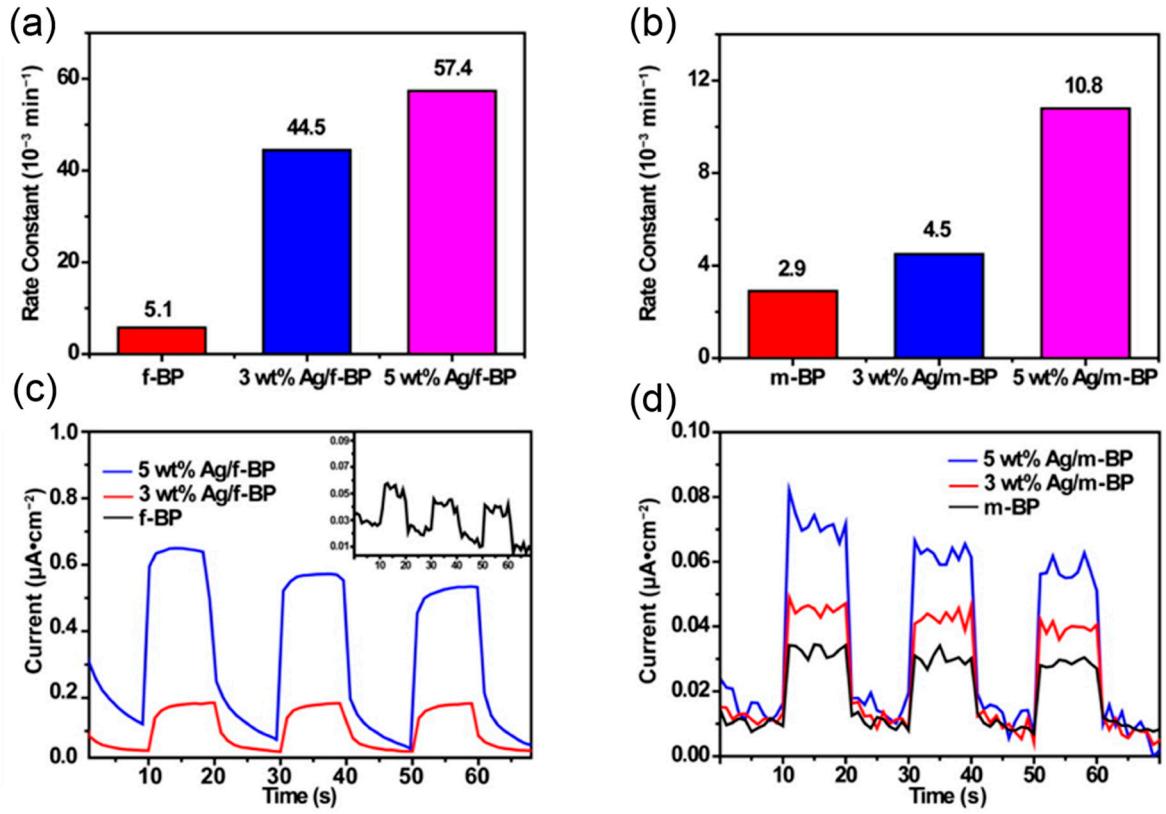

Figure 28. Photoactivity of (**a**) f-BP nanosheets and Ag/f-BP nanohybrids and (**b**) m-BP nanosheets and Ag/m-BP nanohybrids for RhB degradation under visible light illumination. Photocurrent responses of (**c**) f-BP nanosheets and Ag/f-BP nanohybrids and (**d**) m-BP nanosheets and Ag/m-BP nanohybrids. Reprinted with permission from ref. [85]. Copyright © 2020 American Chemical Society.

5.6. Gold

S. C. Warren et al. devised a model photocatalytic system for studying the reduction of chloro(trimethylphosphine)gold (I) ($ClAuPPh_3$) to Au NPs by triethylamine (TEA) mediated by 2D BP [86], where the latter was, at the same time, the substrate for nanoparticles growth and the photocatalyst able to promote the redox process. The nanohybrid Au/2D BP might be considered as a product of the catalytic process itself. Au NPs began to grow on the surface of 2D BP when 2D BP,

TEA, and $ClAuPPh_3$ were combined in *N*-methyl pyrrolidone and exposed to light illumination (see Figure 29).

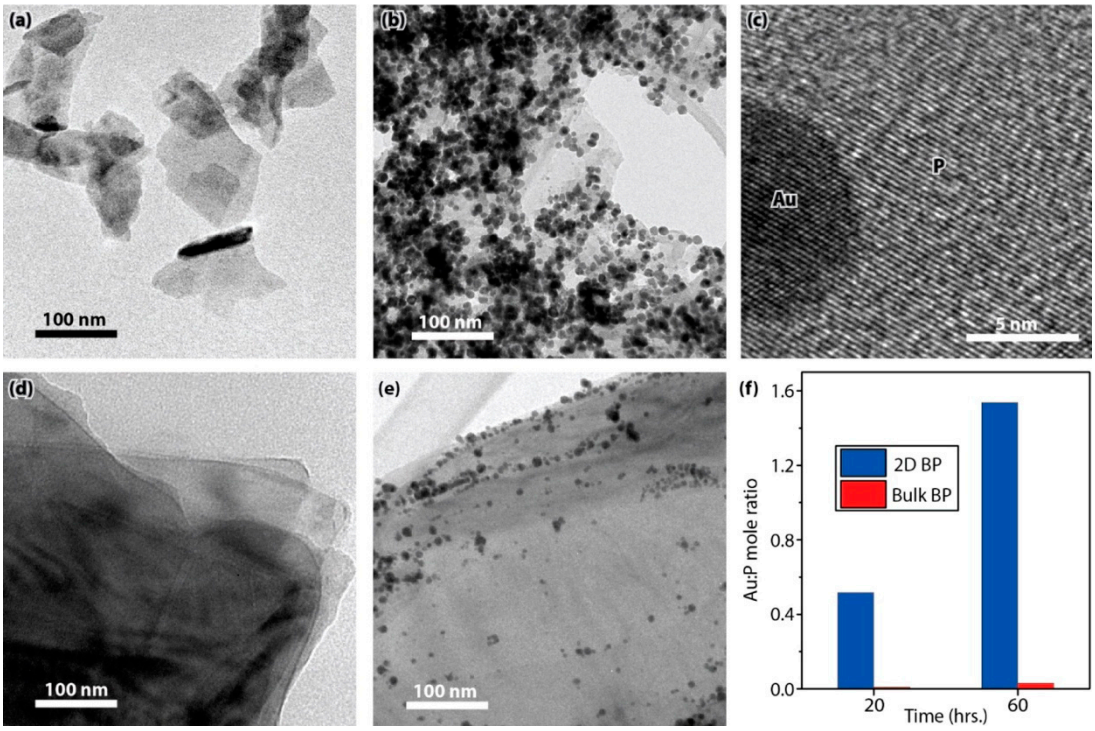

Figure 29. (**a**) Low resolution TEM image of 2D BP. (**b**) 2D BP with Au NPs after 20 h of reaction. (**c**) HRTEM image of the same material. (**d**) Low resolution TEM image of bulk BP. (**e**) Bulk BP with Au NPs after 20 h of reaction. (**f**) The mole ratio of Au:P in the final products after 20 or 60 h. Reprinted with permission from ref. [86]. Copyright © 2020 American Chemical Society.

A control experiment only employing 2D BP and $ClAuPPh_3$ showed how the reaction took place to a much less extent in the absence of TEA, highlighting that 2D BP was not a simple sacrificial reductant for Au(I). Thus, in standard reaction conditions, the electrons that reduced Au (I) must come from TEA. The basic mechanism is believed to be the following: one electron in the valence band of 2D BP is promoted to the conduction band and then transferred to Au (I), reducing it to Au (0). However, the hole left in the valence band of 2D BP must be combined with an electron coming from TEA, which is oxidized regenerating the neutrality in 2D BP, in order for the process to sustain itself (see Figure 30a).

The authors focused on the nanosizing effect that was observed moving from bulk BP to 2D BP. Indeed, bulk BP was almost inactive and its Au (0)/P mole ratio was ≈40 times smaller when compared to 2D BP (see Figure 29f). All of these findings, combined with those of further measurements, can be summarized in the diagram that is shown in Figure 30b.

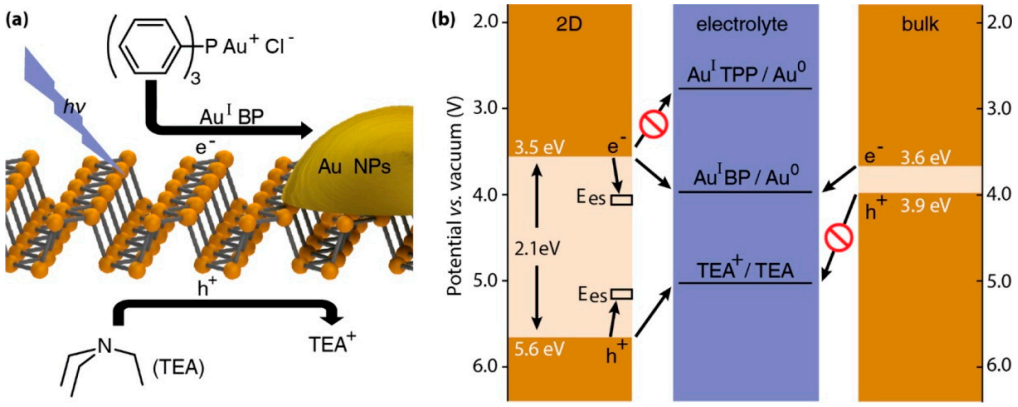

Figure 30. (**a**) Light-driven redox reactions on two-dimensional (2D) BP. $ClAuPPh_3$ (denoted Au^ITPP) is converted to Au^IBP and reduced to Au nanoparticles (NPs), while triethylamine (TEA) is oxidized to TEA^+. (**b**) An energy diagram shows the band edges of monolayer (2D) and bulk BP, redox potentials of each couple, and an indication of whether charge transfer is energetically favorable. The line accompanying Au^ITPP/Au^0 is not a formal reduction potential; rather, it marks the onset of an irreversible reduction of Au^ITPP to Au^0. Reprinted with permission from ref. [86]. Copyright © 2020, American Chemical Society.

Wang F. et al. studied the application of Au NPs-decorated BP as a heterogeneous catalyst some years later [87]. In detail, the reduction of 4-nitrophenol (4-NP) to 4-aminophenol (4-AP) mediated by $NaBH_4$ was the model reaction. Aminophenols are important building blocks in the pharmaceutical industry, as underlined in Section 5.3. The Au NPs/BP nanohybrid was prepared following the published protocol [88], where Au NPs were grown from aqueous $HAuCl_4$ using 2D BP playing both as reducing agent and as support. By this method, nanohybrids with different metal loadings and featuring different NPs size were prepared. The sample with a molar fraction of Au equal to 10%, with average nanoparticles dimension ~5 nm, turned out to be the most effective in 4-NP reduction (see Figure 31A).

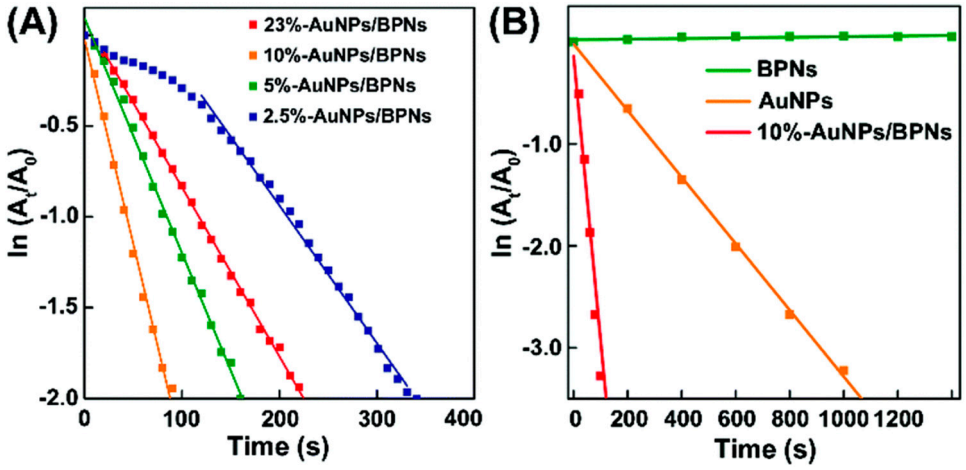

Figure 31. (**A**) Varied catalytic performances of different *x*-AuNPs/BP nanohybrids as revealed by time-dependent absorbance changes of 4-NP (λ = 400 nm). (**B**) Comparative time-dependent absorbance changes of 4-NP upon introducing pristine 2D BP, bare Au NPs or 10%-AuNPs/BP nanohybrids into the 4-NP/$NaBH_4$ mixtures. A_t refers to the absorbance of 4-NP at the indicated time while A_0 refers to the original absorbance of 4-NP. Reprinted with permission from ref. [87]. Copyright © 2020 Royal Society of Chemistry.

The authors demonstrated that anchoring Au NPs to 2D BP not only increased their activity (see Figure 31B), but 10%-AuNPs/BP outperformed many previously reported Au-based catalysts, as shown in Table 1. The improved activity for Au/BP was mainly ascribed to the electron-richness of Au NPs when supported on 2D BP, which donates electron density to the metal, thus enhancing its activity.

Table 1. Comparison of the catalytic activity of 10%-Au/BP nanohybrid with other Au-based catalysts. Adapted from Ref. [87].

Catalyst	TOF (h^{-1})	Reference
Au/Graphene Hydrogel	11.4	[89]
Au/PMMA	90	[90]
AuNPs@CNs	109	[91]
10%-Au/BP	3380	This work

Zhu M. et al. prepared the ternary system BP-Au/$La_2Ti_2O_7$ (BP-Au/LTO) by the simple addition of 2D BP nanosheets to an Au/LTO suspension and treating the resulting dispersion with ultrasounds [92]. The isolated BP-Au/LTO turned out to be an excellent photocatalyst for H_2 production from water in the presence of methanol (20 vol %). When compared to its single components, the ternary heterostructure showed much higher activity under visible light illumination and allowed for extending the photocatalytic activity to embrace the near-infrared region, reaching H_2 production rates of 0.74 and 0.30 mmol g^{-1} h^{-1} at wavelengths longer than 420 and 780 nm, respectively. To unravel the reason behind such extended photoresponse, time-resolved diffuse reflectance spectroscopy was measured and it revealed efficient interfacial electron transfer from excited BP and Au to LTO, which is in agreement with the observed activity, being superior to recently published data shown in Sections 4.1 and 5.4 [56,58,59,84]. This opens the possibility of application of BP to challenging processes based on solar-energy conversion.

6. Conclusions and Perspectives

After the discovery of exfoliated black phosphorus in 2014, its application in heterogeneous catalysis has flourished in the past few years and continues to grow exponentially. Satisfyingly, the exploitation of exfoliated black phosphorus either pristine or as a support for metal nanoparticles has shown advantages in comparison to known (2D-based) catalysts, with BP also being eco-benign. Although being affected by ambient degradation, it has shown superior stability after surface coordination with metals or functionalization, either covalent or not, with organic molecules. This allows for the heterogeneous catalysts based on BP to be stable and recycled, retaining its activity. BP functionalized with the suitable transition metal nanoparticles has shown high selectivity in relevant chemical processes, as catalytic hydrogenation of organic substrates. Additionally, being a natural semiconductor, its application as photocatalyst in the hydrogen evolution/oxygen evolution reaction has already given highly promising results in comparison to benchmark catalysts. Thus, BP can be foreseen as an excellent candidate for future applications in solar-driven water splitting reaction and in other photocatalytic processes, as, for instance, CO_2 reduction and organic pollutant degradation. The key point to make it feasible and extend from laboratory scale to commercial level remains a facile and large scale production of exfoliated BP, from which we are still far away.

Author Contributions: Writing—original draft preparation, M.V.; M.S.-R.; M.P.; writing—review and editing, M.C. All authors have read and agreed to the published version of the manuscript.

Funding: This research was funded by EC through the project PHOSFUN "Phosphorene functionalization: a new platform for advanced multifunctional materials" (ERC ADVANCED GRANT N. 670173 to M.P.). The authors acknowledge the project Ginseng "Graphene related INnovative 2D materials for Sustainable ENerGetIcs and catalysis" for financial support. Italian Ministry for University and Research (MIUR) is acknowledged for funding the project PRIN 2017 KFY7XF FERMAT "Fast ElectRon dynamics in novel hybrid-2D MATerials".

Conflicts of Interest: The authors declare no conflict of interest.

References

1. Grazianetti, C.; Martella, C.; Molle, A. The Xenes Generations: A Taxonomy of Epitaxial Single-Element 2D Materials. *Phys. Status Solidi RRL* **2019**, *14*, 1900439. [CrossRef]
2. Manzeli, S.; Ovchinnikov, D.; Pasquier, D.; Yazyev, O.V.; Kis, A. 2D transition metal dichalcogenides. *Nat. Rev. Mater.* **2017**, *2*, 17033. [CrossRef]
3. Anasori, B.; Lukatskaya, M.R.; Gogotsi, Y. 2D metal carbides and nitrides (MXenes) for energy storage. *Nat. Rev. Mater.* **2017**, *2*, 16098. [CrossRef]
4. Xie, L.M. Two-dimensional transition metal dichalcogenide alloys: Preparation, characterization and applications. *Nanoscale* **2015**, *7*, 18392–18401. [CrossRef]
5. Bridgman, P.W. Two new modifications of phosphorus. *J. Am. Chem. Soc.* **1914**, *36*, 1344–1363. [CrossRef]
6. Li, L.; Yu, Y.; Ye, G.J.; Ge, Q.; Ou, X.; Wu, H.; Feng, D.; Chen, X.H.; Zhang, Y. Black phosphorus field-effect transistors. *Nat. Nanotechnol.* **2014**, *9*, 372–377. [CrossRef]
7. Liu, H.; Neal, A.T.; Zhu, Z.; Luo, Z.; Xu, X.; Tománek, D.; Ye, P.D. Phosphorene: An Unexplored 2D Semiconductor with a High Hole Mobility. *ACS Nano* **2014**, *8*, 4033–4041. [CrossRef]
8. Batmunkh, M.; Bat-Erdene, M.; Shapter, J.G. Black Phosphorus: Synthesis and Application for Solar Cells. *Adv. Energy Mater.* **2017**, *8*, 1701832. [CrossRef]
9. Liu, H.; Hu, K.; Yan, D.; Chen, R.; Zou, Y.; Liu, H.; Wang, S. Recent Advances on Black Phosphorus for Energy Storage, Catalysis, and Sensor Applications. *Adv. Mater.* **2018**, *30*, 1800295. [CrossRef] [PubMed]
10. Li, B.; Lai, C.; Zeng, G.; Huang, D.; Qin, L.; Zhang, M.; Cheng, M.; Liu, X.; Yi, H.; Zhou, C.; et al. Black Phosphorus, a Rising Star 2D Nanomaterial in the Post-Graphene Era: Synthesis, Properties, Modifications, and Photocatalysis Applications. *Small* **2019**, *15*, e1804565. [CrossRef] [PubMed]
11. Carvalho, A.; Wang, M.; Zhu, X.; Rodin, A.; Su, H.; Neto, A.H.C. Phosphorene: From theory to applications. *Nat. Rev. Mater.* **2016**, *1*, 16061. [CrossRef]
12. Jiang, J.-W.; Park, H. Negative poisson's ratio in single-layer black phosphorus. *Nat. Commun.* **2014**, *5*, 4727. [CrossRef] [PubMed]
13. Du, H.; Lin, X.; Xu, Z.; Chu, D. Recent developments in black phosphorus transistors. *J. Mater. Chem. C* **2015**, *3*, 8760–8775. [CrossRef]
14. Hyun, C.; Kim, J.H.; Lee, J.-Y.; Lee, G.-H.; Kim, K.S. Atomic scale study of black phosphorus degradation. *RSC Adv.* **2020**, *10*, 350–355. [CrossRef]
15. Tan, W.C.; Wang, L.; Feng, X.; Chen, L.; Huang, L.; Huang, X.; Ang, K.-W. Recent Advances in Black Phosphorus-Based Electronic Devices. *Adv. Electron. Mater.* **2018**, *5*, 1800666. [CrossRef]
16. Li, P.; Zhang, D.; Liu, J.; Chang, H.; Sun, Y.; Yin, N. Air-Stable Black Phosphorus Devices for Ion Sensing. *ACS Appl. Mater. Interfaces* **2015**, *7*, 24396–24402. [CrossRef]
17. Donarelli, M.; Ottaviano, L.; Giancaterini, L.; Fioravanti, G.; Perrozzi, F.; Cantalini, C. Exfoliated black phosphorus gas sensing properties at room temperature. *2D Mater.* **2016**, *3*, 025002. [CrossRef]
18. Miao, J.; Cai, L.; Zhang, S.; Nah, J.; Yeom, J.; Wang, C. Air-Stable Umidity Sensor Using Few-Layer Black Phosphorus. *ACS Appl. Mater. Interfaces* **2017**, *9*, 10019–10026. [CrossRef]
19. Huang, M.; Wang, M.; Chen, C.; Ma, Z.; Li, X.; Han, J.; Wu, Y. Broadband Black-Phosphorus Photodetectors with High Responsivity. *Adv. Mater.* **2016**, *28*, 3481–3485. [CrossRef]
20. Viti, L.; Hu, J.; Coquillat, D.; Knap, W.; Tredicucci, A.; Politano, A.; Vitiello, M.S. Black Phosphorus Terahertz Photodetectors. *Adv. Mater.* **2015**, *27*, 5567–5572. [CrossRef]
21. Viti, L.; Politano, A.; Zhang, K.; Vitiello, M.S. Thermoelectric terahertz photodetectors based on selenium-doped black phosphorus flakes. *Nanoscale* **2019**, *11*, 1995–2002. [CrossRef] [PubMed]
22. Latiff, N.M.; Teo, W.Z.; Sofer, Z.; Fisher, A.C.; Pumera, M. The Cytotoxicity of Layered Black Phosphorus. *Chem. A Eur. J.* **2015**, *21*, 13991–13995. [CrossRef] [PubMed]
23. Qu, G.; Xia, T.; Zhou, W.; Zhang, X.; Zhang, H.; Hu, L.; Shi, J.; Yu, X.; Jiang, G. Property–Activity Relationship of Black Phosphorus at the Nano–Bio Interface: From Molecules to Organisms. *Chem. Rev.* **2020**, *120*, 2288–2346. [CrossRef] [PubMed]
24. Wang, H.; Yang, X.; Shao, W.; Chen, S.; Xie, J.; Zhang, X.; Wang, J.; Xie, Y. Ultrathin Black Phosphorus Nanosheets for Efficient Singlet Oxygen Generation. *J. Am. Chem. Soc.* **2015**, *137*, 11376–11382. [CrossRef] [PubMed]

25. Raucci, M.G.; Fasolino, I.; Caporali, M.; Serrano-Ruiz, M.; Soriente, A.; Peruzzini, M.; Ambrosio, L. Exfoliated Black Phosphorus Promotes in Vitro Bone Regeneration and Suppresses Osteosarcoma Progression through Cancer-Related Inflammation Inhibition. *ACS Appl. Mater. Interfaces* **2019**, *11*, 9333–9342. [CrossRef]
26. Ienco, A.; Manca, G.; Peruzzini, M.; Mealli, C. Modelling strategies for the covalent functionalization of 2D phosphorene. *Dalton Trans.* **2018**, *47*, 17243–17256. [CrossRef]
27. Brown, A.; Rundqvist, S. Refinement of the crystal structure of black phosphorus. *Acta Crystallogr.* **1965**, *19*, 684–685. [CrossRef]
28. Lange, S.; Schmidt, P.; Nilges, T. Au3SnP7@Black Phosphorus: An Easy Access to Black Phosphorus. *Inorg. Chem.* **2007**, *46*, 4028. [CrossRef]
29. Köpf, M.; Eckstein, N.; Pfister, D.; Grotz, C.; Krüger, I.; Greiwe, M.; Hansen, T.; Kohlmann, H.; Nilges, T. Access and in situ growth of phosphorene-precursor black phosphorus. *J. Cryst. Growth* **2014**, *405*, 6–10. [CrossRef]
30. Wang, J.; Liu, D.; Huang, H.; Yang, N.; Yu, B.; Wen, M.; Wang, X.; Chu, P.K.; Yu, X. In-Plane Black Phosphorus/Dicobalt Phosphide Heterostructure for Efficient Electrocatalysis. *Angew. Chem. Int. Ed.* **2018**, *57*, 2600–2604. [CrossRef]
31. Serrano-Ruiz, M.; Caporali, M.; Ienco, A.; Piazza, V.; Heun, S.; Peruzzini, M. The Role of Water in the Preparation and Stabilization of High-Quality Phosphorene Flakes. *Adv. Mater. Interfaces* **2015**, *3*, 1500441. [CrossRef] [PubMed]
32. Li, Q.; Zhou, Q.; Shi, L.; Chen, Q.; Wang, J. Recent advances in oxidation and degradation mechanisms of ultrathin 2D materials under ambient conditions and their passivation strategies. *J. Mater. Chem. A* **2019**, *7*, 4291–4312. [CrossRef]
33. Pei, J.; Gai, X.; Yang, J.; Wang, X.; Yu, Z.; Choi, D.-Y.; Luther-Davies, B.; Lu, Y. Producing air-stable monolayers of phosphorene and their defect engineering. *Nat. Commun.* **2016**, *7*, 10450. [CrossRef] [PubMed]
34. Bolognesi, M.; Moschetto, S.; Trapani, M.; Prescimone, F.; Ferroni, C.; Manca, G.; Ienco, A.; Borsacchi, S.; Caporali, M.; Muccini, M.; et al. Noncovalent Functionalization of 2D Black Phosphorus with Fluorescent Boronic Derivatives of Pyrene for Probing and Modulating the Interaction with Molecular Oxygen. *ACS Appl. Mater. Interfaces* **2019**, *11*, 22637–22647. [CrossRef] [PubMed]
35. Gusmão, R.; Sofer, Z.; Pumera, M. Functional Protection of Exfoliated Black Phosphorus by Noncovalent Modification with Anthraquinone. *ACS Nano* **2018**, *12*, 5666–5673. [CrossRef]
36. Caporali, M.; Serrano-Ruiz, M.; Telesio, F.; Heun, S.; Nicotra, G.; Spinella, C.; Peruzzini, M. Decoration of exfoliated black phosphorus with nickel nanoparticles and its application in catalysis. *Chem. Commun.* **2017**, *53*, 10946–10949. [CrossRef]
37. Abellán, G.; Wild, S.; Lloret, V.; Scheuschner, N.; Gillen, R.; Mundloch, U.; Maultzsch, J.; Varela, M.; Hauke, F.; Hirsch, A. Fundamental Insights into the Degradation and Stabilization of Thin Layer Black Phosphorus. *J. Am. Chem. Soc.* **2017**, *139*, 10432–10440. [CrossRef]
38. Matthews, P.D.; Hirunpinyopas, W.; Lewis, D.J.; Brent, J.; McNaughter, P.D.; Zeng, N.; Thomas, A.; O'Brien, P.; Derby, B.; Bissett, M.A.; et al. Black phosphorus with near-superhydrophobic properties and long-term stability in aqueous media. *Chem. Commun.* **2018**, *54*, 3831–3834. [CrossRef]
39. Kou, L.; Frauenheim, T.; Chen, C. Phosphorene as a Superior Gas Sensor: Selective Adsorption and Distinct I–V Response. *J. Phys. Chem. Lett.* **2014**, *5*, 2675–2681. [CrossRef]
40. Ou, P.; Song, P.; Liu, X.; Song, J. Superior Sensing Properties of Black Phosphorus as Gas Sensors: A Case Study on the Volatile Organic Compounds. *Adv. Theory Simul.* **2018**, *2*, 1800103. [CrossRef]
41. Huang, Y.; Qiao, J.; He, K.; Bliznakov, S.; Sutter, E.; Chen, X.; Luo, D.; Meng, F.; Su, D.; Decker, J.; et al. Interaction of Black Phosphorus with Oxygen and Water. *Chem. Mater.* **2016**, *28*, 8330–8339. [CrossRef]
42. Abbas, A.N.; Liu, B.; Chen, L.; Ma, Y.; Cong, S.; Aroonyadet, N.; Köpf, M.; Nilges, T.; Zhou, C. Black Phosphorus Gas Sensors. *ACS Nano* **2015**, *9*, 5618–5624. [CrossRef] [PubMed]
43. Lei, S.Y.; Yu, Z.Y.; Shen, H.-Y.; Sun, X.L.; Wan, N.; Yu, H. CO Adsorption on Metal-Decorated Phosphorene. *ACS Omega* **2018**, *3*, 3957–3965. [CrossRef] [PubMed]
44. Lee, G.; Jung, S.; Jang, S.; Kim, J. Platinum-functionalized black phosphorus hydrogen sensors. *Appl. Phys. Lett.* **2017**, *110*, 242103. [CrossRef]
45. Appl, M. *Ammonia: Principles and Industrial Practice*; Wiley-VCH: Hoboken, NJ, USA, 2007; ISBN 978-3-527-61388-5.

46. Erisman, J.W.; Sutton, M.A.; Galloway, J.; Klimont, Z.; Winiwarter, W. How a century of ammonia synthesis changed the world. *Nat. Geosci.* **2008**, *1*, 636–639. [CrossRef]
47. De Klerk, A. *Fischer-Tropsch Refining*; Wiley-VCH: Hoboken, NJ, USA, 2011; ISBN 9783527326051.
48. Mahmoudi, H.; Mahmoudi, M.; Doustdar, O.; Jahangiri, H.; Tsolakis, A.; Gu, S.; LechWyszynski, M. A review of Fischer Tropsch synthesis process, mechanism, surface chemistry and catalyst formulation. *Biofuels Eng.* **2017**, *2*, 11–31. [CrossRef]
49. Tanimu, A.; Alhooshani, K. Advanced Hydrodesulfurization Catalysts: A Review of Design and Synthesis. *Energy Fuels* **2019**, *33*, 2810–2838. [CrossRef]
50. Coker, A.K. Petroleum Refining Design and Applications Handbook. *Pet. Refin. Des. Appl. Handb.* **2018**, *1*, 305–338.
51. Liu, X.; Dai, L. Carbon-based metal-free catalysts. *Nat. Rev. Mater.* **2016**, *1*, 16064. [CrossRef]
52. Abellán, G.; Lloret, V.; Mundloch, U.; Marcia, M.; Neiss, C.; Görling, A.; Varela, M.; Hauke, F.; Hirsch, A. Noncovalent Functionalization of Black Phosphorus. *Angew. Chem. Int. Ed.* **2016**, *55*, 14557–14562. [CrossRef]
53. Wu, W.; Zhang, Z.; Lei, Z.; Wang, X.; Tan, Y.; Cheng, N.; Sun, X. Encapsulating Pt Nanoparticles inside a Derived Two-Dimensional Metal–Organic Frameworks for the Enhancement of Catalytic Activity. *ACS Appl. Mater. Interfaces* **2020**, *12*, 10359–10368. [CrossRef]
54. Zhu, J.; Hu, L.; Zhao, P.; Lee, L.Y.S.; Wong, K.-Y. Recent Advances in Electrocatalytic Hydrogen Evolution Using Nanoparticles. *Chem. Rev.* **2019**, *120*, 851–918. [CrossRef] [PubMed]
55. Mayorga-Martinez, C.C.; Latiff, N.M.; Eng, A.Y.S.; Sofer, Z.; Pumera, M. Black Phosphorus Nanoparticle Labels for Immunoassays via Hydrogen Evolution Reaction Mediation. *Anal. Chem.* **2016**, *88*, 10074–10079. [CrossRef]
56. Zhu, X.; Zhang, T.; Sun, Z.; Chen, H.; Guan, J.; Chen, X.; Ji, H.; Du, P.; Yang, S. Black Phosphorus Revisited: A Missing Metal-Free Elemental Photocatalyst for Visible Light Hydrogen Evolution. *Adv. Mater.* **2017**, *29*, 1605776. [CrossRef] [PubMed]
57. Rahman, M.Z.; Kwong, C.W.; Davey, K.; Qiao, S. 2D phosphorene as a water splitting photocatalyst: Fundamentals to applications. *Energy Environ. Sci.* **2016**, *9*, 709–728. [CrossRef]
58. Muduli, S.K.; Varrla, E.; Xu, Y.; Kulkarni, S.A.; Katre, A.; Chakraborty, S.; Chen, S.; Sum, T.C.; Xu, R.; Mathews, N. Evolution of hydrogen by few-layered black phosphorus under visible illumination. *J. Mater. Chem. A* **2017**, *5*, 24874–24879. [CrossRef]
59. You, H.; Jia, Y.; Wu, Z.; Wang, F.; Huang, H.; Wang, Y. Room-temperature pyro-catalytic hydrogen generation of 2D few-layer black phosphorene under cold-hot alternation. *Nat. Commun.* **2018**, *9*, 2889. [CrossRef]
60. Jiang, Q.; Xu, L.; Chen, N.; Zhang, H.; Dai, L.; Wang, S. Facile Synthesis of Black Phosphorus: An Efficient Electrocatalyst for the Oxygen Evolving Reaction. *Angew. Chem. Int. Ed.* **2016**, *55*, 13849–13853. [CrossRef]
61. Ren, X.; Zhou, J.; Qi, X.; Liu, Y.; Huang, Z.; Li, Z.; Ge, Y.; Dhanabalan, S.C.; Ponraj, J.S.; Wang, S.; et al. Few-Layer Black Phosphorus Nanosheets as Electrocatalysts for Highly Effcient Oxygen Evolution Reaction. *Adv. Energy Mater.* **2017**, *7*, 1700396. [CrossRef]
62. Shi, F.; Huang, K.; Wang, Y.; Zhang, W.; Li, L.; Wang, X.; Feng, S. Black Phosphorus-Modified Co3O4 through Tuning the Electronic Structure for Enhanced Oxygen Evolution Reaction. *ACS Appl. Mater. Interfaces* **2019**, *11*, 17459–17466. [CrossRef]
63. Fryzuk, M.D.; Johnson, S. The continuing story of dinitrogen activation. *Co ord. Chem. Rev.* **2000**, *200*, 379–409. [CrossRef]
64. Légaré, M.-A.; Bélanger-Chabot, G.; Dewhurst, R.D.; Welz, E.; Krummenacher, I.; Engels, B.; Braunschweig, H. Nitrogen fixation and reduction at boron. *Science* **2018**, *359*, 896–900. [CrossRef]
65. Zhang, L.; Chen, G.-F.; Ding, L.-X.; Wang, H. Advanced Non-metallic Catalysts for Electrochemical Nitrogen Reduction under Ambient Conditions. *Chem. Eur. J.* **2019**, *25*, 12464–12485. [CrossRef]
66. Zhang, L.; Ding, L.-X.; Chen, G.-F.; Yang, X.; Wang, H. Ammonia Synthesis Under Ambient Conditions: Selective Electroreduction of Dinitrogen to Ammonia on Black Phosphorus Nanosheets. *Angew. Chem. Int. Ed.* **2019**, *58*, 2612–2616. [CrossRef]
67. Lloret, V.; Rivero-Crespo, M.; Vidal-Moya, J.A.; Wild, S.; Doménech-Carbó, A.; Heller, B.S.J.; Shin, S.; Steinrück, H.-P.; Maier, F.; Hauke, F.; et al. Few layer 2D pnictogens catalyze the alkylation of soft nucleophiles with esters. *Nat. Commun.* **2019**, *10*, 509. [CrossRef]
68. Trost, B.M.; Van Vranken, D.L. Asymmetric Transition Metal-Catalyzed Allylic Alkylations. *Chem. Rev.* **1996**, *96*, 395–422. [CrossRef]

69. Sueki, S.; Kuninobu, Y. Copper-Catalyzed N- and O-Alkylation of Amines and Phenols using Alkylborane Reagents. *Org. Lett.* **2013**, *15*, 1544–1547. [CrossRef]
70. Shi, F.; Geng, Z.; Huang, K.; Liang, Q.; Zhang, Y.; Sun, Y.; Cao, J.; Feng, S. Cobalt Nanoparticles/Black Phosphorus Nanosheets: An Efficient Catalyst for Electrochemical Oxygen Evolution. *Adv. Sci.* **2018**, *5*, 1800575. [CrossRef]
71. Oger, C.; Balas, L.; Durand, T.; Galano, J.-M. ChemInform Abstract: Are Alkyne Reductions Chemo-, Regio-, and Stereoselective Enough To Provide Pure (Z)-Olefins in Polyfunctionalized Bioactive Molecules? *Chem. Rev.* **2013**, *44*, 1313–1350. [CrossRef]
72. Delgado, J.A.; Benkirane, O.; Claver, C.; Curulla-Ferré, D.; Godard, C. Advances in the preparation of highly selective nanocatalysts for the semi-hydrogenation of alkynes using colloidal approaches. *Dalton Trans.* **2017**, *46*, 12381–12403. [CrossRef]
73. Chen, Y.; Li, C.; Zhou, J.; Zhang, S.; Rao, D.; He, S.; Wei, M.; Evans, D.G.; Duan, X. Metal Phosphides Derived from Hydrotalcite Precursors toward the Selective Hydrogenation of Phenylacetylene. *ACS Catal.* **2015**, *5*, 5756–5765. [CrossRef]
74. Li, C.; Chen, Y.; Zhang, S.; Zhou, J.; Wang, F.; He, S.; Wei, M.; Evans, D.G.; Duan, X. Nickel-Gallium Intermetallic Nanocrystal Catalysts in the Semihydrogenation of Phenylacetylene. *ChemCatChem* **2014**, *6*, 824–831. [CrossRef]
75. Erokhin, A.V.; Lokteva, E.; Yermakov, A.; Boukhvalov, D.; Maslakov, K.I.; Golubina, E.V.; Uimin, M. Phenylacetylene hydrogenation on Fe@C and Ni@C core–shell nanoparticles: About intrinsic activity of graphene-like carbon layer in H2 activation. *Carbon* **2014**, *74*, 291–301. [CrossRef]
76. Vanni, M.; Serrano-Ruiz, M.; Telesio, F.; Heun, S.; Banchelli, M.; Matteini, P.; Mio, A.M.; Nicotra, G.; Spinella, C.; Caporali, S.; et al. Black Phosphorus/Palladium Nanohybrid: Unraveling the Nature of P–Pd Interaction and Application in Selective Hydrogenation. *Chem. Mater.* **2019**, *31*, 5075–5080. [CrossRef]
77. Orlandi, M.; Brenna, D.; Harms, R.; Jost, S.; Benaglia, M. Recent Developments in the Reduction of Aromatic and Aliphatic Nitro Compounds to Amines. *Org. Process. Res. Dev.* **2016**, *22*, 430–445. [CrossRef]
78. Kovacic, P.; Somanathan, R. Nitroaromatic compounds: Environmental toxicity, carcinogenicity, mutagenicity, therapy and mechanism. *J. Appl. Toxicol.* **2014**, *34*, 810–824. [CrossRef]
79. Costantino, F.; Nocchetti, M.; Bastianini, M.; Lavacchi, A.; Caporali, M.; Liguori, F. Robust Zirconium Phosphate–Phosphonate Nanosheets Containing Palladium Nanoparticles as Efficient Catalyst for Alkynes and Nitroarenes Hydrogenation Reactions. *ACS Appl. Nano Mater.* **2018**, *1*, 1750–1757. [CrossRef]
80. Wu, T.; Fan, J.; Li, Q.; Shi, P.; Xu, Q.; Min, Y. Palladium Nanoparticles Anchored on Anatase Titanium Dioxide-Black Phosphorus Hybrids with Heterointerfaces: Highly Electroactive and Durable Catalysts for Ethanol Electrooxidation. *Adv. Energy Mater.* **2017**, *8*, 1701799. [CrossRef]
81. Wu, T.; Ma, Y.; Qu, Z.-B.; Fan, J.; Li, Q.; Shi, P.; Xu, Q.; Min, Y. Black Phosphorus–Graphene Heterostructure-Supported Pd Nanoparticles with Superior Activity and Stability for Ethanol Electro-oxidation. *ACS Appl. Mater. Interfaces* **2019**, *11*, 5136–5145. [CrossRef]
82. Bai, L.; Wang, X.; Tang, S.; Kang, Y.; Wang, J.; Yu, Y.; Zhou, Z.-K.; Ma, C.; Zhang, X.; Jiang, J.; et al. Black Phosphorus/Platinum Heterostructure: A Highly Efficient Photocatalyst for Solar-Driven Chemical Reactions. *Adv. Mater.* **2018**, *30*, e1803641. [CrossRef]
83. Wang, X.; Bai, L.; Lu, J.; Zhang, X.; Liu, D.; Yang, H.; Wang, J.; Chu, P.K.; Ramakrishna, S.; Yu, X.F. Rapid Activation of Platinum with Black Phosphorus for Efficient Hydrogen Evolution. *Angew. Chem. Int. Ed.* **2019**, *58*, 19060–19066. [CrossRef]
84. Tian, B.; Tian, B.; Smith, B.; Scott, M.C.; Lei, Q.; Hua, R.; Tian, Y.; Liu, Y. Facile bottom-up synthesis of partially oxidized black phosphorus nanosheets as metal-free photocatalyst for hydrogen evolution. *Proc. Natl. Acad. Sci. USA* **2018**, *115*, 4345–4350. [CrossRef]
85. Lei, W.; Zhang, T.; Liu, P.; Rodriguez, J.A.; Liu, G.; Liu, M.-H. Bandgap- and Local Field-Dependent Photoactivity of Ag/Black Phosphorus Nanohybrids. *ACS Catal.* **2016**, *6*, 8009–8020. [CrossRef]
86. Hu, J.; Guo, Z.; McWilliams, P.E.; Darges, J.E.; Druffel, D.; Moran, A.M.; Warren, S. Band Gap Engineering in a 2D Material for Solar-to-Chemical Energy Conversion. *Nano Lett.* **2015**, *16*, 74–79. [CrossRef]
87. Wu, Q.; Liang, M.; Zhang, S.; Liu, X.; Wang, F. Development of functional black phosphorus nanosheets with remarkable catalytic and antibacterial performance. *Nanoscale* **2018**, *10*, 10428–10435. [CrossRef]
88. Huang, H.; Xiao, Q.; Wang, J.; Yu, X.; Wang, H.; Zhang, H.; Chu, P.K. Black phosphorus: A two-dimensional reductant for in situ nanofabrication. *npj 2D Mater. Appl.* **2017**, *1*, 20. [CrossRef]

89. Liu, Y.; Li, J.; Liu, C.-Y. Au/graphene hydrogel: Synthesis, characterization and its use for catalytic reduction of 4-nitrophenol. *J. Mater. Chem.* **2012**, *22*, 8426. [CrossRef]
90. Kuroda, K.; Ishida, T.; Haruta, M. Reduction of 4-nitrophenol to 4-aminophenol over Au nanoparticles deposited on PMMA. *J. Mol. Catal. A Chem.* **2009**, *298*, 7–11. [CrossRef]
91. Wu, X.; Lu, C.; Zhou, Z.; Yuan, G.; Xiong, R.; Zhang, X. Green synthesis and formation mechanism of cellulose nanocrystal-supported gold nanoparticles with enhanced catalytic performance. *Environ. Sci. Nano* **2014**, *1*, 71. [CrossRef]
92. Zhu, M.; Cai, X.; Fujitsuka, M.; Zhang, J.; Majima, T. Au/La2Ti2O7Nanostructures Sensitized with Black Phosphorus for Plasmon-Enhanced Photocatalytic Hydrogen Production in Visible and Near-Infrared Light. *Angew. Chem. Int. Ed.* **2017**, *56*, 2064–2068. [CrossRef]